SPECT and PET Myocardial Perfusion Imaging: Tracers and Techniques

4

Vasken Dilsizian

The application of a radiotracer technique to measure physiologic parameters, such as pulmonary circulation, dates back to 1927. Despite considerable advances in the application of radiotracer technique for interrogating physiologic and pathophysiologic cardiopulmonary conditions in the early twentieth century, the spatial resolution of the scintigraphic instruments used to measure tracer concentration in the heart, lungs, and blood was limited. The advent of single-photon emission CT (SPECT) in the late 1970s and positron emission tomography (PET) in the 1980s dramatically changed the clinical utility of radiotracer technique for the assessment of myocardial perfusion, viability, and function.

Both SPECT and PET technologies use similar reconstruction processes to obtain tomographic images of the heart. However, they differ in the type of radiopharmaceuticals and kind of instrumentation used to acquire cardiac images. SPECT allows a noninvasive evaluation of myocardial blood flow by extractable tracers such as ^{201}Tl- and ^{99m}Tc-labeled perfusion tracers. PET, on the other hand, allows a noninvasive assessment of regional blood flow, function, and metabolism using physiologic substrates prepared with positron-emitting isotopes such as carbon, oxygen, nitrogen, and fluorine (Fig. 4.1, Table 4.1). Radioisotopes commonly used with SPECT emit γ-rays of varying energies and have relatively long physical half-lives. The localization of γ-rays emitted by single-photon–emitting radiotracers in the heart is conventionally accomplished by an Anger scintillation camera (gamma camera), which converts the γ-rays to light photons via sodium iodide scintillation detectors. The gamma camera limits the direction of photons entering the detector by a collimator and then positions each event electronically. More recently, new designs of high-speed SPECT cameras have been introduced, which utilize a series of small, pixilated solid-state detector columns with cadmium zinc telluride or CSI (Tl) crystals, which provide considerably more information for each detected γ-ray. In addition, the design of the solid-state detector design with wide-angle tungsten collimators combined with a novel image reconstruction algorithm provide true three-dimensional, patient-specific images localized to the heart. Compared with the conventional SPECT cameras, the high-speed SPECT systems can provide up to an eightfold increase in count rates, thereby reducing imaging times significantly from 14–15 minutes with a conventional Anger camera to 5–6 minutes with the newer solid-state cameras, while achieving a twofold increase in spatial resolution, from 9 to 12 mm for Anger cameras to 4.3–4.9 mm for cadmium zinc telluride cameras. The radioisotopes used for optimal scintigraphic registration with SPECT cameras are limited to those that emit γ-rays with an energy range that is suitable for the gamma camera and related single-photon devices, such as ^{201}Tl, ^{99m}Tc, and ^{123}I. Although clinically useful, estimates of relative myocardial blood flow by SPECT are significantly affected by attenuation artifacts that are not reliably corrected for when compared with PET attenuation-correction algorithms.

V. Dilsizian (✉)
University of Maryland School of Medicine, Baltimore, MD, USA
e-mail: vdilsizian@umm.edu

V. Dilsizian, J. Narula (eds.), *Atlas of Nuclear Cardiology*, https://doi.org/10.1007/978-3-030-49885-6_4

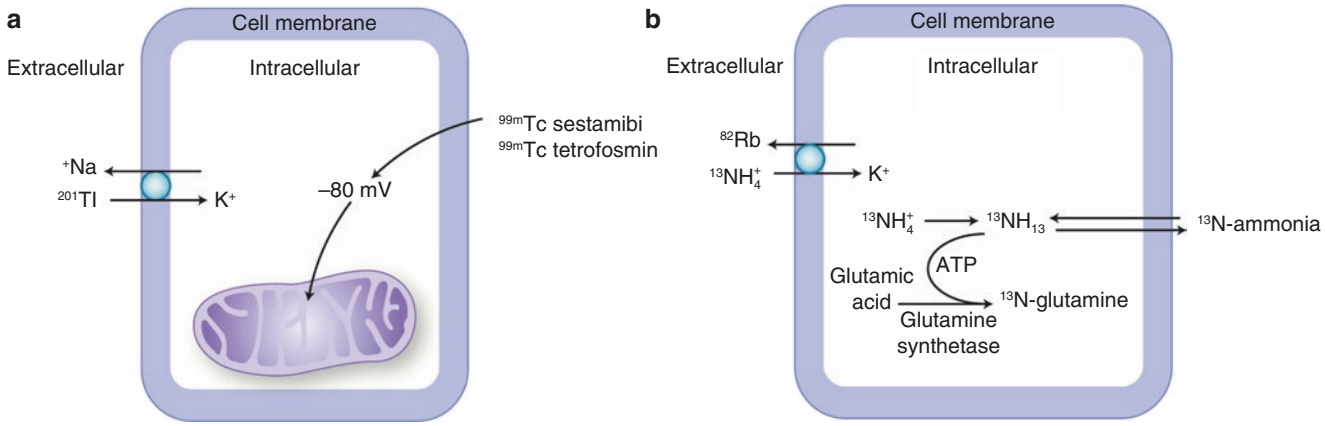

Fig. 4.1 Properties of flow tracers used for single-photon emission computed tomography (SPECT) (**a**) and positron emission tomography (PET) (**b**). To reflect regional myocardial perfusion, radiotracers commonly used with SPECT and PET must have high extraction by the heart and rapid clearance from the blood. Clinically available radiopharmaceuticals that meet these criteria for SPECT are ^{201}Tl, ^{99m}Tc-labeled sestamibi, and tetrofosmin; for PET, ^{82}Rb and ^{13}N-ammonia. If radiotracers are not highly extracted (<50%) or if the residence time in the blood is prolonged (clearance half-time of >5 minutes), they cannot be used to assess regional perfusion

Tracer	Mechanism of myocyte uptake	Usual dose, *mCi*
Properties of SPECT flow tracers		
^{201}Tl	Na–K ATPase—sarcolemma	2–3
^{99m}Tc-sestamibi	Negative transmembrane potential—mitochondria	8–40
^{99m}Tc-tetrofosmin	Negative transmembrane potential—mitochondria	8–40
Properties of PET flow tracers		
^{82}Rb	Na–K ATPase—sarcolemma	30–60
^{13}N ammonia	Trapped as ^{13}N-glutamine (mediated by ATP)—cytoplasm	10–20

Table 4.1 Properties of SPECT and PET flow tracers

Positron-emitting radioisotopes commonly used with PET emit two γ-rays, 511 keV each, and have relatively short physical half-lives. When the high-energy positron is emitted from a nucleus, it travels a short distance and collides with an electron. The result is complete annihilation of both the positron and the electron, and the conversion of the combined mass to energy in the form of electromagnetic radiation (two γ-rays, 511 keV energy each). Because the γ-rays are perfectly collinear (discharged at 180° to each other) and travel in opposite directions, the PET detectors can be programmed to register only events with a temporal coincidence of photons that strike directly at opposing detectors. This results in improved spatial (4–6 mm) and temporal resolution. Moreover, the PET system is more sensitive than a SPECT system (higher count rate) and provides a more robust soft tissue attenuation correction. The consequence of these advantages with PET is the possibility for quantitation of the tracer concentration in absolute units.

Myocardial Perfusion, Uptake, and Clearance

Regional myocardial blood flow is critically dependent on the driving pressure gradient and the resistance of the vascular bed. As illustrated in Fig. 4.2, advanced degrees of coronary artery disease may exist at rest without myocardial ischemia, owing to compensatory dilatation of the resistance vessels, and regional myocardial blood flow is preserved in both patent and stenosed coronary artery branches. Such disparity between myocardial blood flow and coronary anatomy attests to the complementary information that a physiologic study such as myocardial perfusion SPECT or PET provides, in addition to information from coronary angiography with CT or diagnostic catheterization. In a canine model, over 80% occlusion of the coronary artery was necessary before ischemia was observed under the basal state. Because the pressure drop across a stenosis varies directly with the length of the stenosis and inversely with the fourth power of the radius (Bernoulli's theorem), resistance almost triples as the severity of coronary artery stenosis increases from 80% to 90%. Consequently, during exercise or pharmacologic stress testing, when the resistance to the distal bed and the pressure distending the stenotic coronary artery declines, myocardial ischemia ensues.

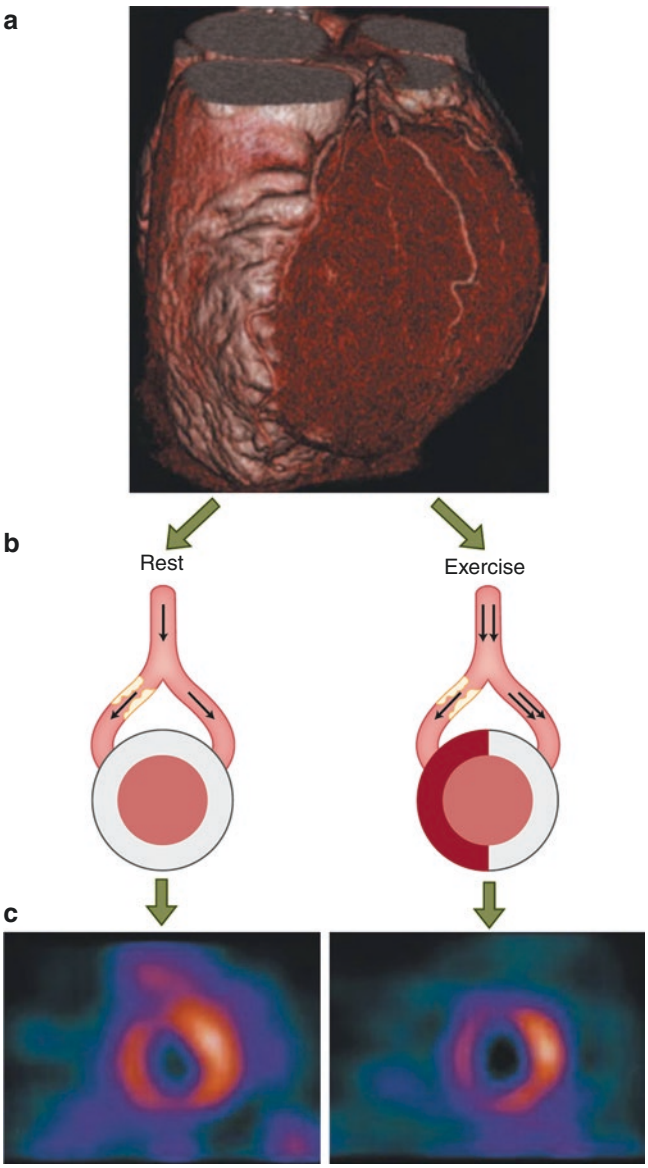

Fig. 4.2 Myocardial blood flow and coronary anatomy: disparate yet complementary information. Advanced degrees of coronary artery disease may exist at rest (**a**) without myocardial ischemia, owing to compensatory dilatation of the resistance vessels. At rest, regional myocardial blood flow is preserved in both patent and stenosed coronary artery branches (**b** and **c**), but during exercise or pharmacologic stress testing, when the resistance to the distal bed and the pressure distending the stenotic coronary artery declines, myocardial ischemia ensues

Coronary blood flow in myocardial regions without coronary artery stenosis may increase about twofold to threefold during vigorous aerobic exercise, but in the setting of moderate-to-severe coronary artery stenosis, the degree of coronary flow increase may be attenuated when compared with myocardial regions without coronary artery stenosis. The insufficient coronary blood flow increase during stress results in impaired perfusion and myocardial ischemia. In patients with coronary artery disease, an inverse relationship has been shown between the increase in myocardial blood flow and the percentage of coronary artery stenosis once the lumen is narrowed by approximately 40–50%. Thus, when a radiotracer such as thallium is injected at peak exercise, the relative differences in regional myocardial blood flow will be reflected in disproportionate concentrations of regional thallium activity on the stress images. Therefore, myocardial perfusion imaging identifies subcritical coronary artery stenosis when it is performed in conjunction with exercise or pharmacologic stress, but not at rest.

The radiotracer that most closely parallels myocardial blood flow would be expected to most accurately identify coronary artery narrowing. There are several classes of radiopharmaceuticals that meet these criteria, such as microspheres, ^{201}Tl, ^{99m}Tc-labeled perfusion tracers, ^{15}O-water, ^{13}N-ammonia, and ^{82}Rb. Differences in the first-pass extraction of these tracers ultimately determine the regional myocardial tracer uptake relative to regional blood flow (Fig. 4.3). The extraction fraction is determined experimentally in a Langendorff preparation and represents first- or single-pass extraction of the radiotracer from the blood into the myocardium. An ideal myocardial perfusion tracer would be expected to exhibit a linear relationship to myocardial blood flow over a wide range of flow rates in mL/g/minute. ^{15}O-water, a PET myocardial flow tracer, exhibits such a relationship. A linear relationship between the tracer uptake and myocardial blood flow would, therefore, differentiate between regions with normal or high blood flow (supplied by normal coronary arteries) and abnormal or low blood flow (supplied by narrowed coronary arteries). However, this is not the case for all other radiotracers commonly used in clinical practice. In an open-chest canine model of regional myocardial ischemia with dipyridamole-induced hyperemia, thallium showed a more ideal linear relationship between the tracer uptake and myocardial blood flow assessed by microspheres when compared with ^{99m}Tc-labeled myocardial perfusion agents. The extraction fraction of ^{201}Tl is high at 85%, whereas the extraction fraction of ^{99m}Tc-sestamibi is only 60% and that of ^{99m}Tc-tetrofosmin is approximately 54%. Beyond the first-pass extraction, recirculation of the radiotracer in patients allows further extraction of the radiotracers from the blood into the myocardium during that particular physiologic state (rest, exercise, pharmacologic, or mental stress).

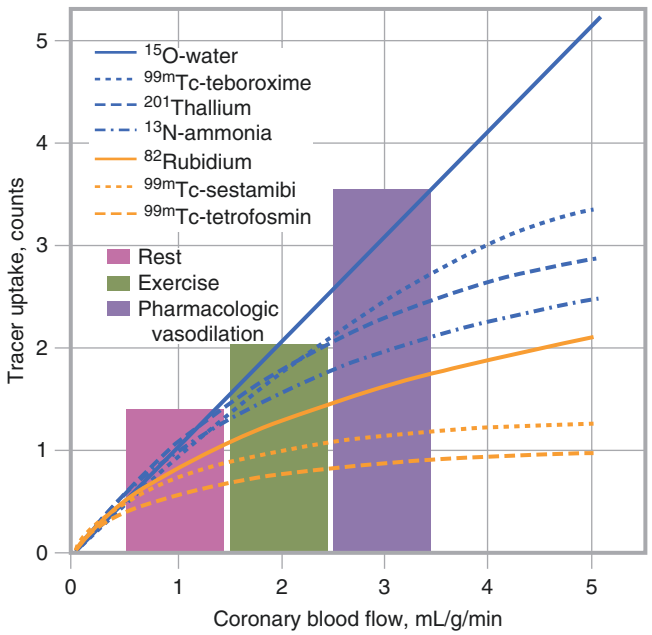

Fig. 4.3 Schematic illustration of radiotracer uptake in relation to regional myocardial blood flow

At rest, myocardial blood flow is approximately 1 mL/g/minute. During physical exercise, myocardial blood flow usually increases two- to threefold, whereas with pharmacologic vasodilation (adenosine, regadenoson, or dipyridamole), myocardial blood flow exceeds 3 mL/g/minute. All clinically available perfusion tracers for SPECT and PET demonstrate "roll-off" at high coronary blood flow levels (a deviation from the line of identity). For SPECT tracers, this "roll-off" phenomenon is particularly marked for ^{99m}Tc-sestamibi and ^{99m}Tc-tetrofosmin, and less so for ^{201}Tl. This implies that at higher flow levels, relative myocardial tracer uptake may underestimate regional myocardial blood flow and thereby also the underlying coronary artery disease. Clinical studies have shown that this underestimation of regional blood flow deficits does not affect the detection of significant (>70%) coronary artery stenosis, but it is important to point out that coronary artery stenosis between 50% and 70% may go undetected, especially with radiotracers with low extraction fraction and marked roll-off phenomenon.

Once a radiotracer is injected intravenously at peak stress, it is extracted rapidly from the blood and accumulated in the myocardium in proportion to regional blood flow. All clinically useful radiotracers have extraction fractions above 50% and are cleared rapidly from the blood in 5–7 minutes after injection (Fig. 4.4). Because ^{201}Tl has a higher first-pass extraction fraction and is cleared more rapidly from the blood than ^{99m}Tc-sestamibi and ^{99m}Tc-tetrofosmin, patients are encouraged to exercise for an additional 1 minute after an injection of ^{201}Tl at peak exercise and for 2 minutes after an injection of ^{99m}Tc-sestamibi or ^{99m}Tc-tetrofosmin at peak exercise. If exercise is stopped too early with the ^{99m}Tc perfusion tracers (that is, 1 minute rather than 2 minutes after an injection), residual radiotracer activity in the blood may be taken up at a different physiologic state (under resting condition), thereby underestimating the presence and extent of myocardial ischemia.

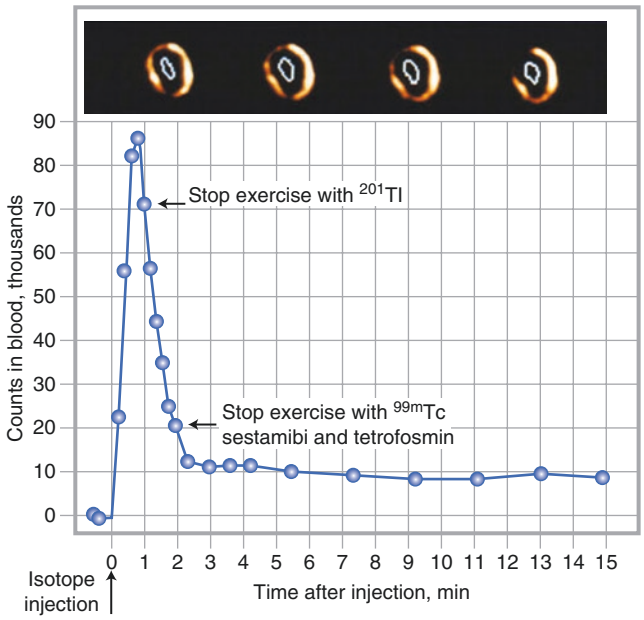

Fig. 4.4 Blood clearance of radiotracers

Image Interpretation and Quantitation

SPECT myocardial perfusion images are interpreted on the basis of the presence, location, extent, and severity of perfusion defects using a standard 17-segment model [1] and visual scoring (Fig. 4.5).

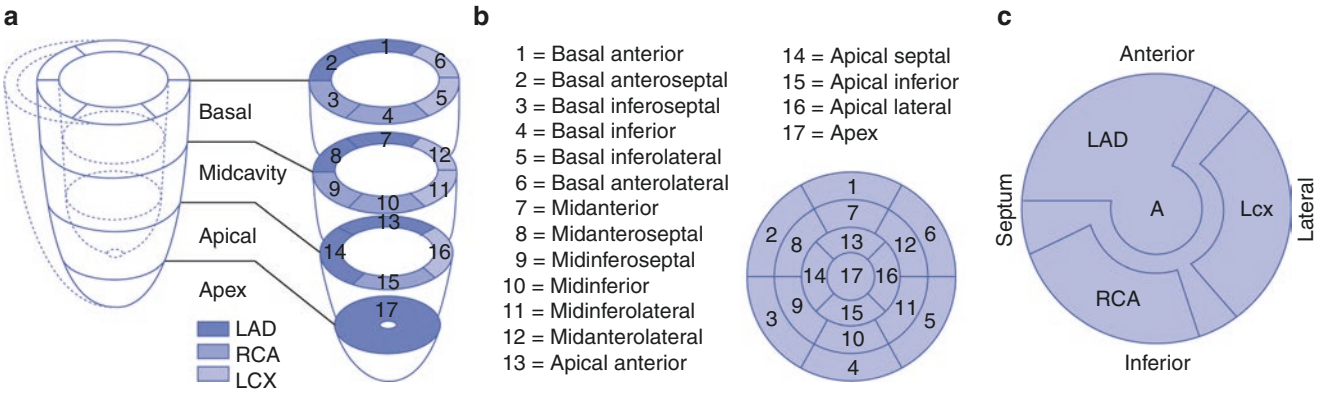

Fig. 4.5 Myocardial segmentation, standard nomenclature, and vascular territories. (**a**) A standard segmentation model divides the left ventricle into three major short-axis slices: apical, midcavity, and basal. The apical short-axis slice is divided into four segments, whereas the midcavity and basal slices are divided into six segments. The apex is analyzed separately, usually from a vertical long-axis slice. Although the anatomy of coronary arteries may vary in individual patients, the anterior, septal, and apical segments are usually ascribed to the left anterior descending (LAD) coronary artery, the inferior and basal septal segments to the right coronary artery (RCA), and the lateral segments to the left circumflex (LCX) coronary artery. The apex can also be supplied by the RCA and LCX arteries. (**b**) Data from the individual short-axis tomograms can be combined to create a bull's-eye polar plot representing a two-dimensional compilation of all the three-dimensional short-axis perfusion data. Standard nomenclature for the 17 segments is outlined. (**c**) The two-dimensional compilation of perfusion data can then easily be assigned to specific vascular territories

Because radionuclide images are intrinsically digital images, the true quantification of tracer uptake in myocardial regions is feasible [2] (Fig. 4.6).

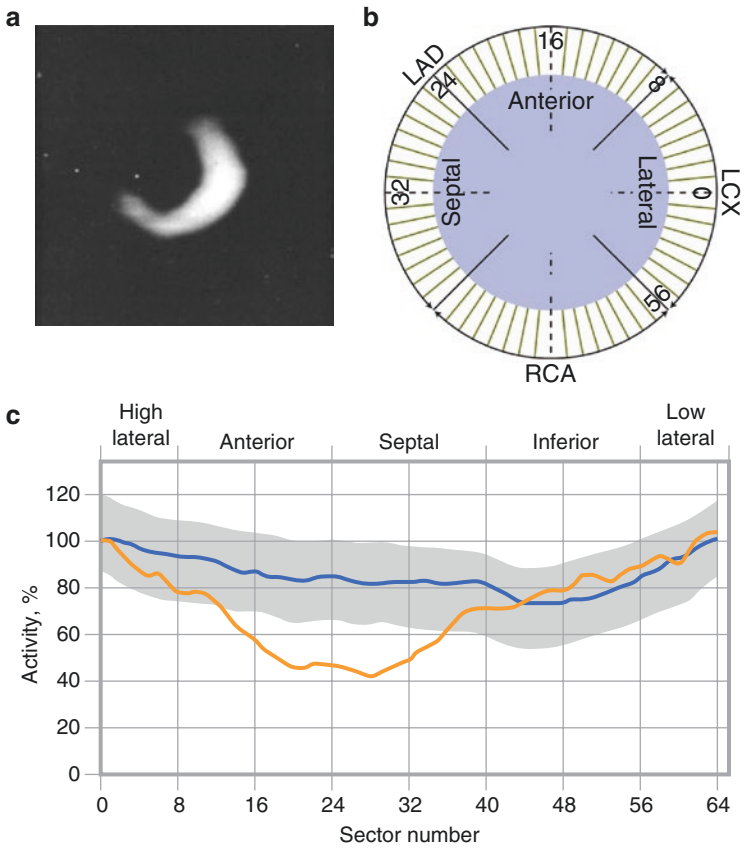

Fig. 4.6 Quantitative analysis of tracer uptake. (**a**) The methodology of semiautomatic quantitative circumferential profile analysis is applied to a short-axis ^{201}Tl tomogram obtained after exercise in a patient with coronary artery disease. (**b**) The left ventricular myocardium is divided into 64 sectors, representing four myocardial regions. (**c**) The patient's thallium uptake during stress imaging in each section (*orange line*) and the normal range (mean ± 2 SD for normal subjects; *shaded area with blue line*). The patient's count profile displays the distribution of counts in the tomogram relative to maximal counts counterclockwise, starting at 0, which represents the high lateral region, which is designated as the normal reference value of 100% (maximal count density). Whenever a region of the circumferential profile falls below the lower limit of normal, that region of the patient's myocardium is considered to have a perfusion defect. In this patient, thallium perfusion defects are apparent in the anterior and septal regions. LAD—left anterior descending; LCX—left circumflex; RCA—right coronary artery

Although normal myocardial perfusion SPECT images appear to have homogeneous radiotracer uptake, regional inhomogeneities are commonly present that are related to normal structural variation, tissue attenuation, and abdominal visceral activity, as well as technical factors associated with image acquisition. During SPECT acquisition, the camera is physically closer to the lateral wall (which is in close proximity to the lateral chest wall) than to the other myocardial regions. Consequently, the lateral region is subject to less soft tissue attenuation and is associated with a more efficient count capture. This should not be interpreted as relative hypoperfusion in all other myocardial regions (which will appear to have slightly less uptake). Thus, in normal SPECT images, the lateral region is usually the area with maximal radiotracer uptake, and it is often difficult to detect subtle perfusion defects visually within the lateral region because the activity of the radiotracer may remain greater than or similar to other myocardial regions. This would especially be the case in patients with multivessel disease, in whom an equivalent reduction in perfusion in several myocardial regions would still result in greater tracer activity in the lateral territory, termed *balanced reduction in flow*. Normal structural variations include the "drop-out" of the upper septum (transition from the muscular to membranous septum) and apical thinning (an anatomically thinner apex may appear as a perfusion defect). Figure 4.7 illustrates common variations and artifacts of myocardial perfusion SPECT.

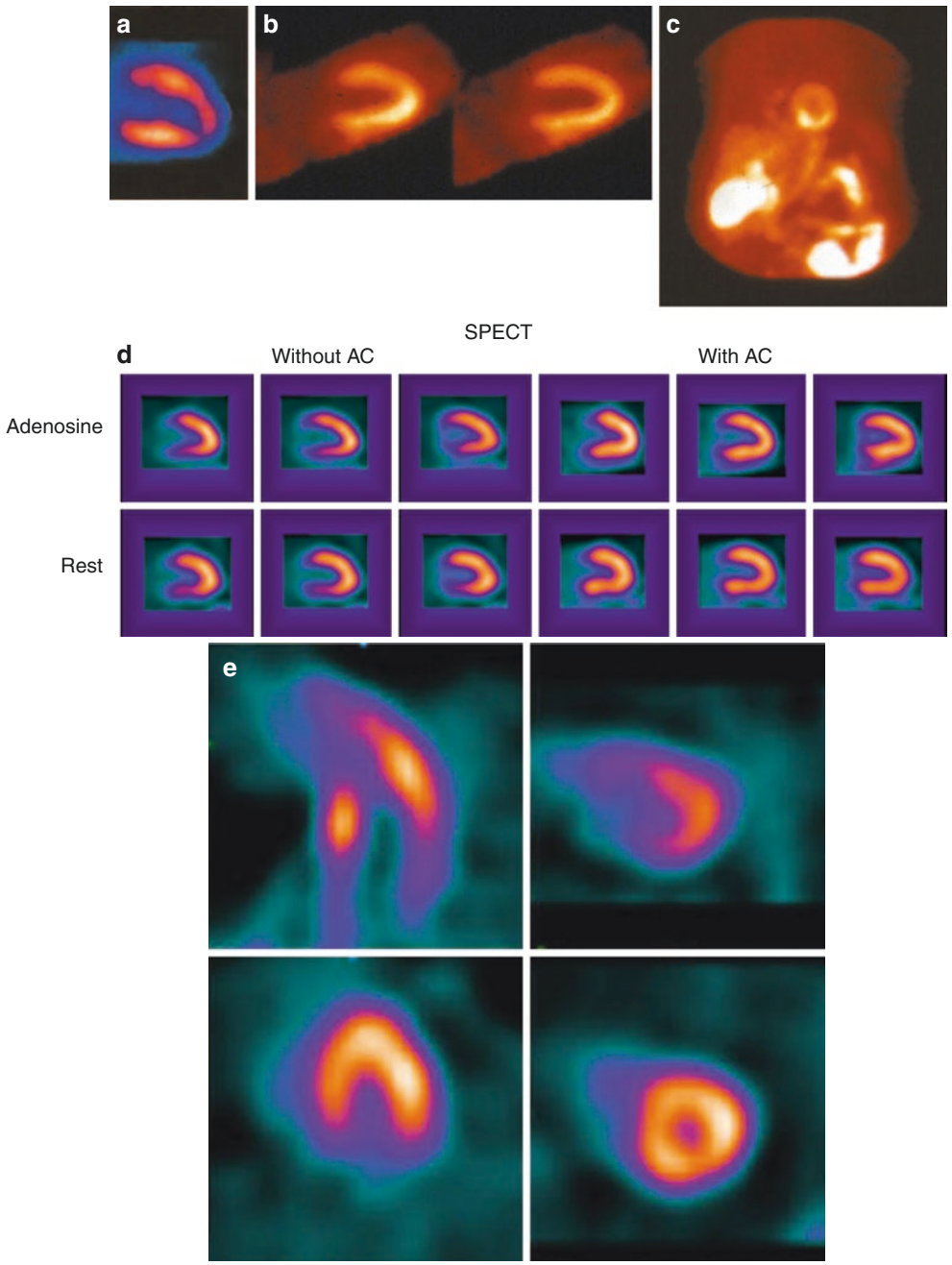

Fig. 4.7 Common variations and artifacts of myocardial perfusion SPECT. (**a**) An example of apical thinning is shown. Soft tissue attenuation can present as breast attenuation, commonly in women with large or dense breasts. (**b**) This figure is an example of a patient with breast attenuation, which shows mildly decreased uptake in the anterior region. (**c**) Breast attenuation can be recognized on the rotating planar projection images as a photopenic shadow over the heart that has the contour of a breast. The demonstration of preserved wall thickening in the anterior region by gated SPECT imaging may be helpful in differentiating an attenuation artifact from myocardial infarction. (**d**) Similarly, inferior wall attenuation can be caused by the diaphragm or by other abdominal visceral structures, such as the liver or bowel, either overlapping or near the inferior wall, or ascites and large pleural effusions. Soft tissue attenuation such as that caused by the diaphragm can be corrected with attenuation correction (AC), but attenuation due to radiotracer activity within abdominal visceral structures, such as the liver or bowel, either overlapping or near the inferior wall, cannot be resolved with an attenuation correction algorithm. Adjacent abdominal visceral activity may falsely increase the number of counts that are assigned within the heart (in which case the adjacent myocardium appears to be "hot") or may cause a "ramp filter" or "negative lobe" artifact (in which case the adjacent myocardium appears to be "cool"). (**e**) This figure is an example of a patient motion artifact exhibiting as a "hurricane sign." Images in the *top row* show the consequence of significant patient motion in creating artifactual regional perfusion defects. In the *bottom row*, when the images are reacquired in the same patient without motion artifact, the distribution of the radiotracer appears homogeneous in all myocardial regions, without regional perfusion defects

An imbalance between oxygen supply (usually due to reduced myocardial perfusion) and oxygen demand (determined primarily by the rate and force of myocardial contraction) is termed *ischemic myocardium*. A clinical presentation of such an imbalance may be symptomatic (angina pectoris) or asymptomatic (silent ischemia). If the oxygen supply–demand imbalance is transient (i.e., triggered by exertion), it represents reversible ischemia. The scintigraphic hallmark of myocardial ischemia is a reversible perfusion defect, as seen in Fig. 4.8.

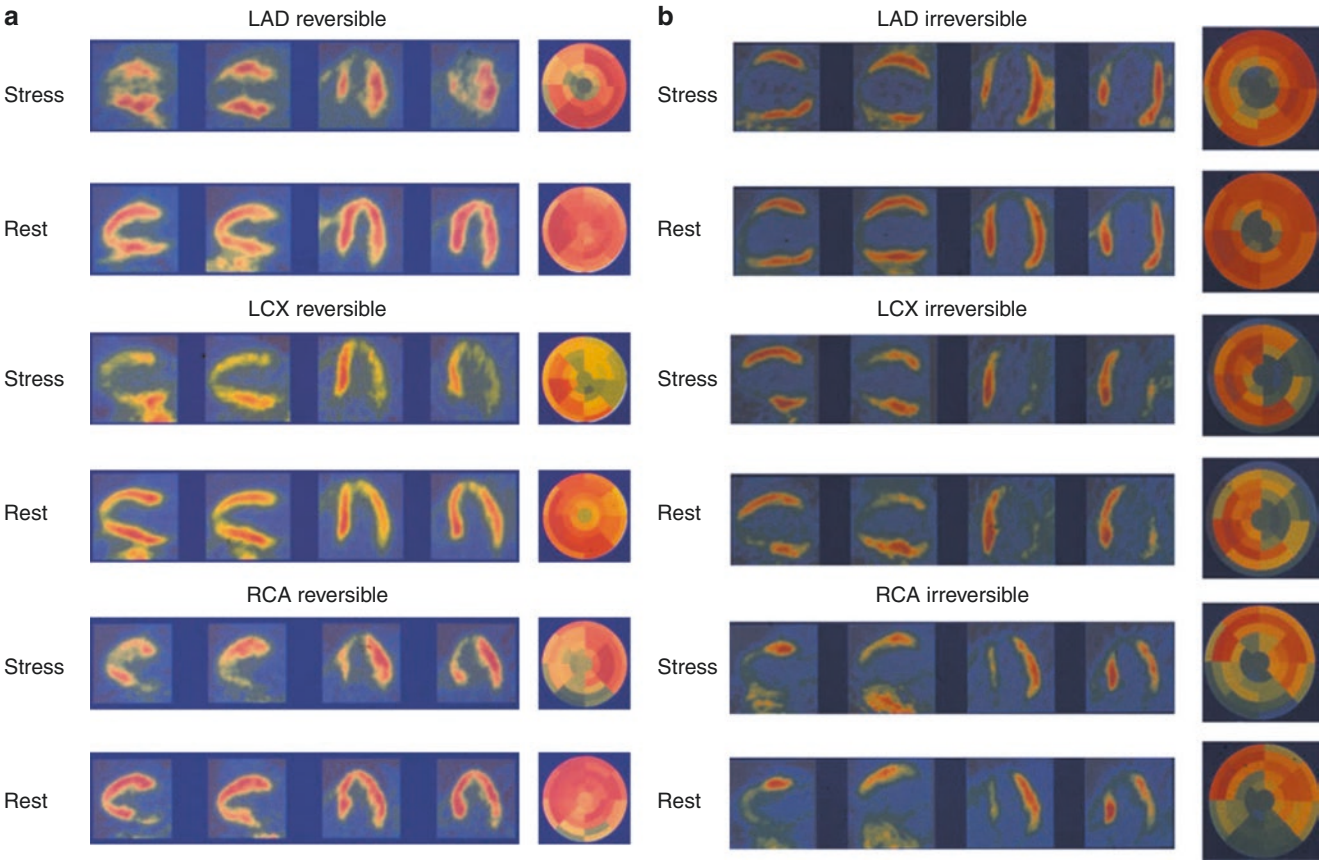

Fig. 4.8 Reversible and irreversible perfusion defects: myocardial ischemia and infarction. (**a**) Examples of reversible perfusion defects (from a transient oxygen supply–demand imbalance, as triggered by exertion) in the left anterior descending (LAD), left circumflex (LCX), and right coronary artery (RCA) territories. On the other hand, if a regional oxygen supply–demand imbalance is prolonged (i.e., during myocardial infarction), high-energy phosphates will be depleted, regional contractile function will progressively deteriorate, and cell membrane rupture with cell death will follow (myocardial infarction). The scintigraphic hallmark of myocardial infarction is a fixed or irreversible perfusion defect. (**b**) Examples of irreversible (fixed) perfusion defects in the LAD, LCX, and RCA territories

Beyond myocardial perfusion, additional important abnormal findings can be present on the rotating planar projection images, which allow the visualization of noncardiac structures such as lung, breast, and the thyroid gland. Findings such as lung uptake, parathyroid adenoma, or lung cancer, shown in Fig. 4.9, should be observed and reported.

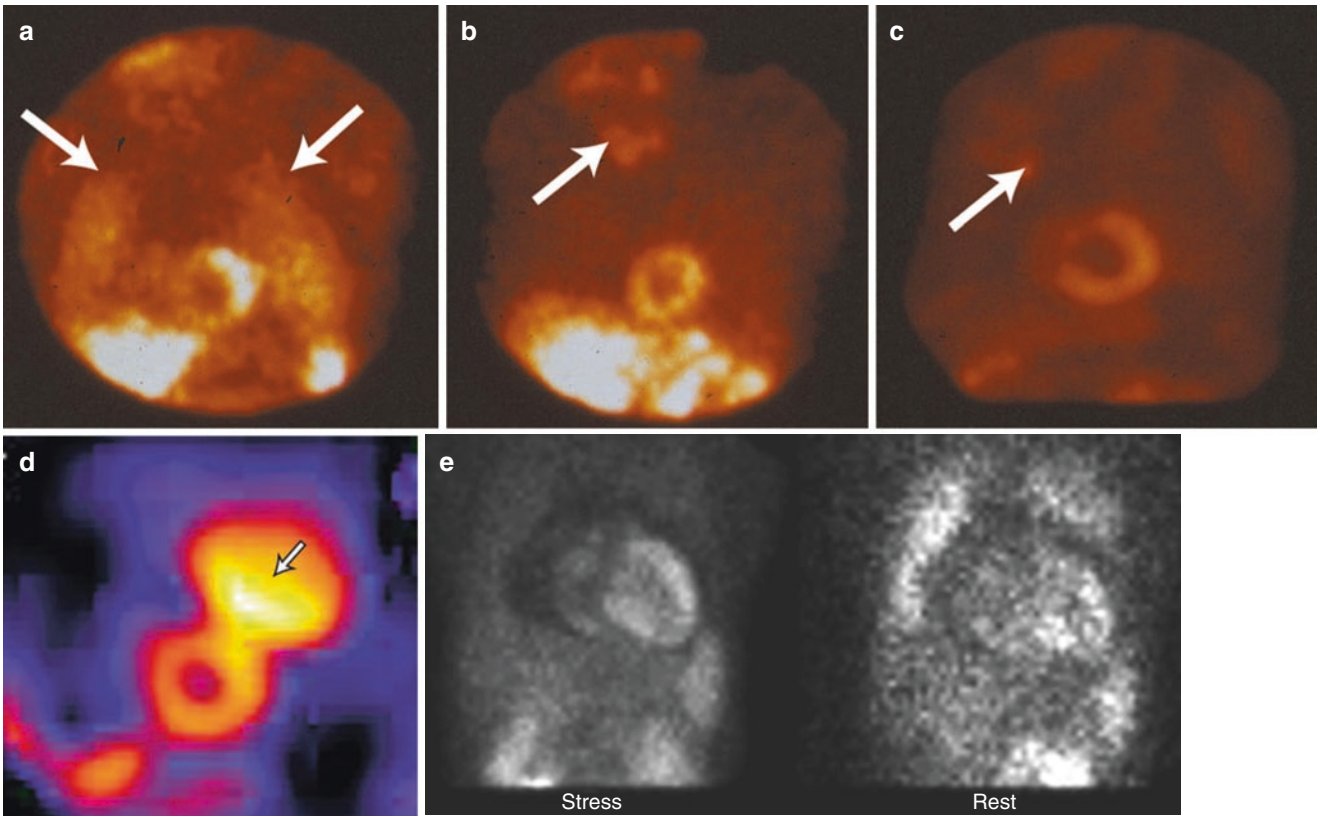

Fig. 4.9 Clinically relevant extracardiac activity. (**a**) Increased lung uptake (*arrows*) is associated with extensive coronary artery disease and an adverse prognosis. In patients with extensive myocardial ischemia and/or left ventricular dysfunction, it is likely that increases in the left atrial and pulmonary capillary wedge pressures slow the pulmonary transit of the radiotracer, thereby allowing more time for extraction or transudation of the radiotracer into the interstitial spaces of the lung. Lung uptake has been more extensively validated with ^{201}Tl than ^{99m}Tc perfusion tracers. Because of differences in the biodistribution and clearance of ^{201}Tl and ^{99m}Tc perfusion tracers, thallium images are acquired within a few minutes after exercise (minimal splanchnic and background activity), but the ^{99m}Tc-sestamibi and ^{99m}Tc-tetrofosmin are usually acquired 15–30 minutes after exercise and 30–60 minutes after pharmacologic vasodilation. (Liver uptake is more prominent than the heart if imaged too early.) Thus, lung uptake, even if it was present early after stress, may be missed with ^{99m}Tc-sestamibi and ^{99m}Tc-tetrofosmin because of the more delayed imaging after stress when compared with thallium. (**b**) An example of a patient with findings of a parathyroid adenoma (*arrow*) in stress ^{99m}Tc-sestamibi myocardial perfusion SPECT. The rotating planar projection images allow the visualization of noncardiac structures such as lung, breast, and the thyroid gland. An abnormal uptake of ^{201}Tl, ^{99m}Tc-sestamibi, and ^{99m}Tc-tetrofosmin in the neck can identify parathyroid adenoma, whereas in the chest they can identify primary lesions such as lung or breast cancer, ectopic parathyroid adenoma, or metastatic lesions. (**c**) Similarly, shown is an example of a patient with findings of a solitary lung nodule (*arrow*) on a stress ^{99m}Tc-sestamibi myocardial perfusion SPECT. (**d**) Intense ^{99m}Tc-sestamibi uptake (*arrow*), superior to the heart, represents an anterior mediastinal mass, which is compatible with thymoma. Thymomas are the most common neoplasm of the anterior mediastinum (representing 20% of all anterior mediastinal masses in the adult population), but their incidence is rather rare, only 0.15/100,000 cases. The differentiation of benign from malignant thymoma cannot be made on the basis of size or intensity of ^{99m}Tc-sestamibi uptake. Additional studies are required to further characterize the lesion. (**e**) Example of a patient with pericardial effusion. A photopenic halo of decreased activity surrounding the entire heart is consistent with pericardial effusion, which could be a consequence of myopericarditis, an infection such as tuberculous pericardial effusion, or a malignant effusion such as breast cancer, melanoma, or lung cancer. (**d** *Courtesy of* Jeffrey R. Folk; **e** *Courtesy of* Rory Hachamovitch)

Extensive literature exists on the diagnostic yield of stress SPECT myocardial perfusion imaging [3–14]. Among 1827 patients referred for the evaluation of chest discomfort (pooled data from 12 studies performed between 1989 and 1999), the overall sensitivity of myocardial perfusion SPECT for the detection of angiographic coronary artery disease was 91%, the specificity was 72%, and the normalcy rate (in subjects with low likelihood for coronary artery disease who did not undergo coronary angiography) was 91% (Fig. 4.10).

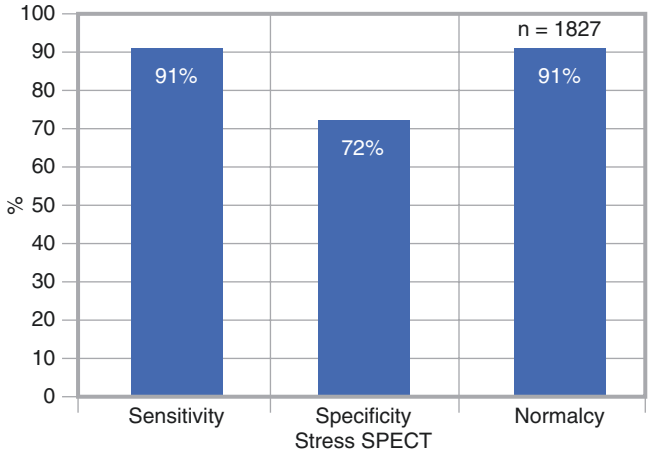

Fig. 4.10 Detection of angiographic coronary artery disease with radiotracers

The clinical indications for stress–rest myocardial perfusion SPECT imaging (Table 4.2) are well established [15]. Most patients are referred because of chest pain symptoms and suspected coronary artery disease (CAD), but patients with known CAD are referred as well. For these patients, the purpose of testing may be to evaluate the effect of therapy or to determine the cause of changes in symptom patterns. In addition, many patients are referred for risk stratification after acute myocardial infarction. Stress–rest SPECT imaging plays an important role in the preoperative evaluation of patients who are scheduled to undergo major noncardiac surgery. The most important and useful clinical application of SPECT myocardial perfusion imaging is to stratify patients into low-risk and high-risk categories and, thus, contribute to the management of patients.

Detection of coronary artery disease
Evaluation of known coronary artery disease
Risk stratification
Preoperative evaluation
Differentiation of viable from scarred myocardium
Assessment of acute chest pain in the emergency department

Table 4.2 Clinical indications for myocardial perfusion imaging

SPECT images should not be interpreted as either normal or abnormal. The prognosis of a patient is related to the degree of myocardial perfusion abnormality. Quantification or semiquantification provides that important prognostic information. Table 4.3 lists findings that characterize high-risk versus low-risk SPECT images. Among the high-risk findings are large perfusion defects in the stress images that involve multiple coronary artery territories. (If two or more coronary territories are involved, the study should be considered to be high-risk.) Large stress-induced reversible defects represent extensive myocardial ischemia, which may be associated with increased lung uptake, transient ischemic left ventricular cavity dilatation, and transient increased right ventricular myocardial visualization.

High risk
Large perfusion defect on stress imaging
Multiple coronary artery territories
Large reversible defects
Increased lung uptake
Transient left ventricular dilatation
Abnormal lung uptake
Left ventricular dysfunction (LVEF < 45%)
Low risk
Normal stress images
Small stress defect
Small regions of defect reversibility

LVEF left ventricular ejection fraction

Table 4.3 High-risk and low-risk SPECT images

One of the strongest features of stress myocardial perfusion SPECT imaging is its ability to identify low-risk patients. Patients with unequivocal normal exercise or pharmacologic stress myocardial perfusion SPECT images exhibit less than a 1% future cardiac event rate, which is the same as the general population. For patients who are in an exercise study, this presumes that the patient achieved greater than 85% of the predicted maximum heart rate for a man or woman of their age. Similarly, presuming that adequate exercise was performed, patients with small myocardial perfusion defects on stress and small regions of defect reversibility have a low risk for future cardiac events, but these patients should be treated aggressively with medical therapy owing to the presence of coronary artery disease. It is important to emphasize that stress myocardial perfusion SPECT images should always be interpreted in conjunction with clinical and electrocardiographic data. For example, a rare patient may have a markedly abnormal exercise portion of the test but normal or near-normal SPECT images. It is the responsibility of the nuclear cardiologist to determine the significance of such disparate data.

SPECT Techniques: ^{201}Tl

Figure 4.11 illustrates a stress-redistribution ^{201}Tl protocol. The initial distribution of ^{201}Tl (early after intravenous injection) is proportional to regional blood flow, but the redistribution phase, the later distribution of ^{201}Tl over a 3- to 4-hour period, is a function of regional blood volume and is unrelated to flow. During the redistribution phase, there is a continuous exchange of ^{201}Tl between the myocardium and the extracardiac compartments, driven by the concentration gradient of the tracer and myocyte viability. Thus, the extent to defect resolution, from the initial to delayed redistribution images over time (a reversible defect), reflects one index of myocardial viability. When only nonviable, scarred myocardium is present, the initial ^{201}Tl defect (an irreversible defect) persists over time without redistribution. When both viable and scarred myocardium are present, ^{201}Tl redistribution is incomplete, giving the appearance of partial reversibility. Thus, the initial phase of ^{201}Tl studies reflects reductions in flow caused by coronary artery narrowing, whereas the delayed, redistribution phase of ^{201}Tl studies reflects myocardial potassium space, differentiating viable from scarred myocardium.

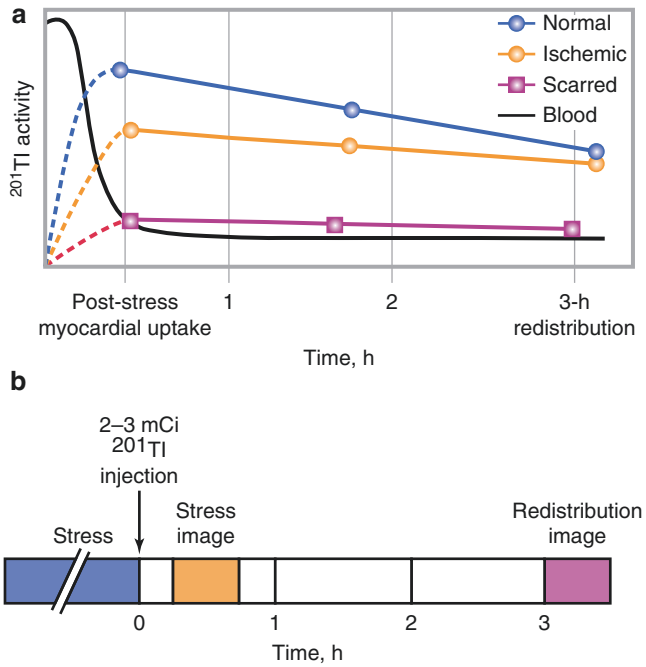

Fig. 4.11 Stress-redistribution ^{201}Tl protocol: Schematic diagrams of ^{201}Tl uptake and redistribution in normal and ischemic myocardium (**a**), and a stress-redistribution protocol (**b**)

Beyond its value as a perfusion and viability tracer, the stress-redistribution ^{201}Tl studies provide useful information regarding patient outcome and prognosis. In patients with chronic ischemic heart disease, an increased lung-to-heart ratio after stress, transient left ventricular cavity dilatation, and extensive reversible and irreversible ^{201}Tl defects have been shown to be important predictors of an adverse outcome. Similarly, the combination of reversible ^{201}Tl defects and increased lung-to-heart ratio has been shown to differentiate between low- and high-risk patients after an acute myocardial infarction. Figure 4.12 demonstrates that ^{201}Tl scintigraphy was much better than an exercise treadmill test or coronary angiography at identifying a low-risk subgroup of patients with acute myocardial infarction.

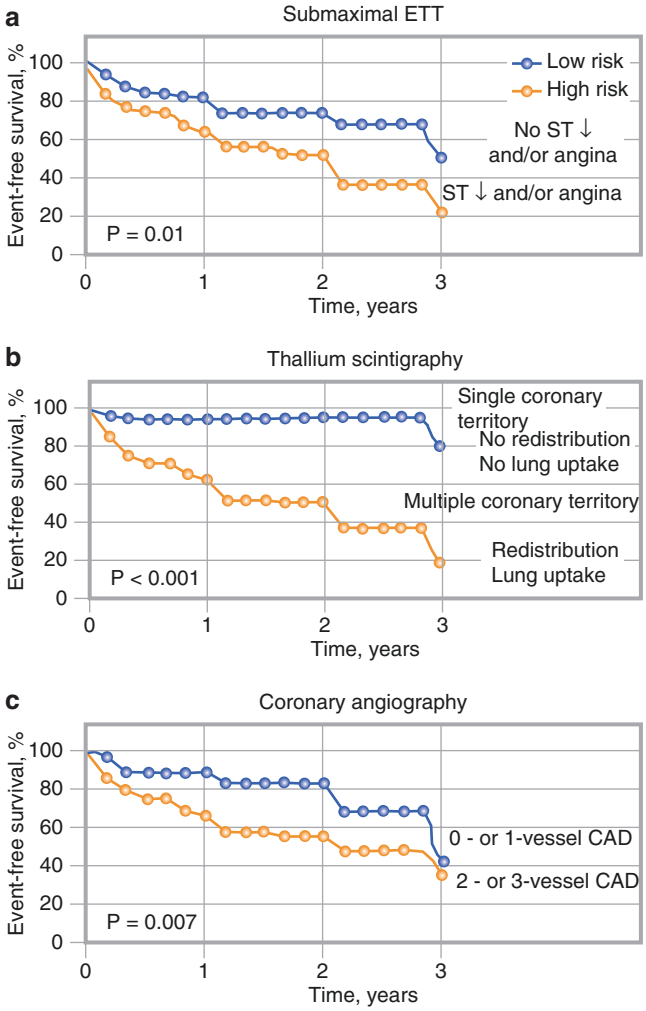

Fig. 4.12 Prognostic value of thallium scintigraphy. Among patients with acute myocardial infarction who had a predischarge submaximal exercise treadmill test (ETT), ^{201}Tl scintigraphy, and coronary angiography, ^{201}Tl identified the low-risk subgroup much better than the submaximal ETT or angiography [16]. CAD—coronary artery disease

In some patients with critically stenosed coronary arteries, the initial uptake of ^{201}Tl in the ischemic region is low and the accumulation of the tracer from the recirculating ^{201}Tl in the blood is slow. Consequently, ischemic but viable myocardium may appear to be irreversible over the 3- to 4-hour redistribution period and may mimic the appearance of scarred myocardium, but if more time is allowed for redistribution, a greater number of viable myocardial regions may be differentiated from scarred myocardium. Figure 4.13 shows a late-redistribution protocol and maps demonstrating the effect of late ^{201}Tl redistribution. However, up to 37% of segments that remained irreversible in both early and late redistribution studies showed an improvement in function after revascularization [17]. Moreover, despite implementing longer imaging time, a number of late redistribution studies had suboptimal count statistics at 24 hours. The data suggest that although late ^{201}Tl imaging improves the identification of viable myocardium when compared with early redistribution imaging, it continues to underestimate segmental improvement after revascularization.

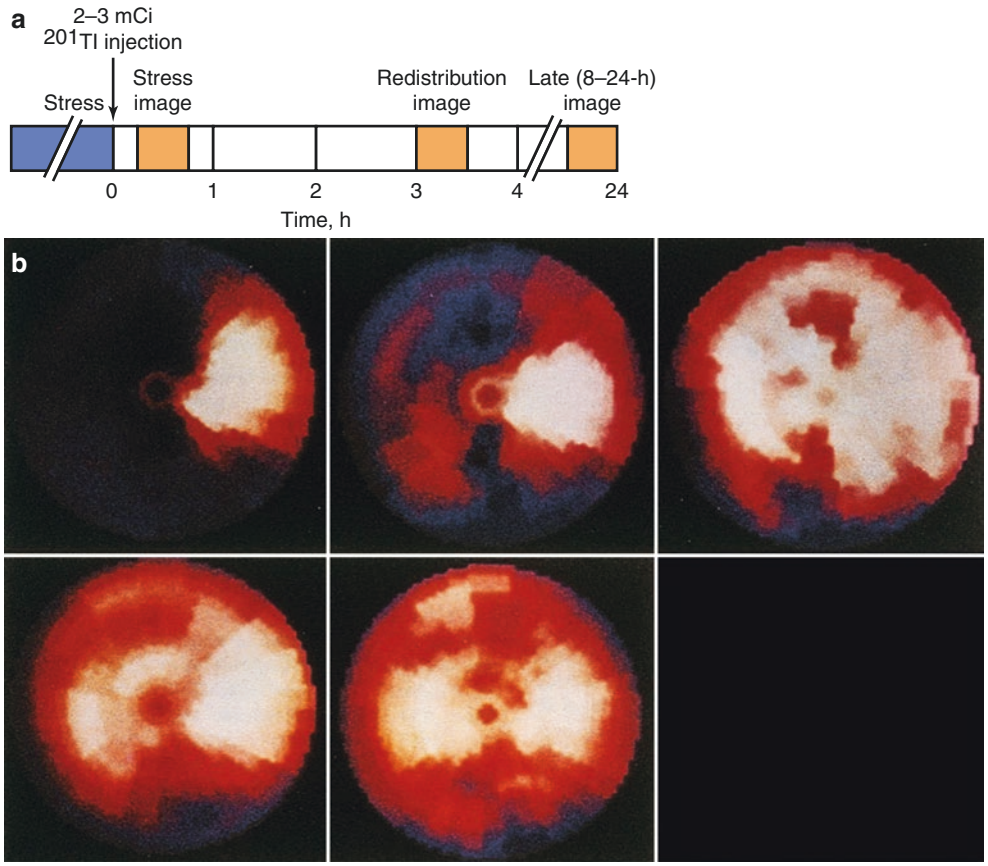

Fig. 4.13 (**a**) Late (24-hour) redistribution protocol after stress-redistribution ^{201}Tl imaging. (**b**) Polar maps demonstrating the effect of late ^{201}Tl redistribution. A bull's-eye image of ^{201}Tl immediately after exercise (*top left*) shows a marked decrease in tracer uptake throughout the anterior, septal, apical, and inferior regions, with partial redistribution in the 4-hour delayed image (*center*). However, in the late (17-hour) redistribution image (*right*), there is complete reversibility in all myocardial regions, which is suggestive of extensive myocardial ischemia rather than a scar. After successful percutaneous transluminal coronary angioplasty, the bull's-eye image of ^{201}Tl immediately after exercise (*bottom left*) shows normal distribution of the tracer throughout all myocardial regions, documenting the accuracy of late redistribution ^{201}Tl and the absence of myocardial scarring. In patients who are treated with revascularization, 95% of segments that demonstrated late redistribution showed improved ^{201}Tl uptake after revascularization. However, as with early (3–4 hour) redistribution, the absence of late redistribution underestimates the presence of viable myocardium (*right*). (**b** *From* Cloninger et al. [18], with permission from Elsevier)

The redistribution of ^{201}Tl is dependent, in part, on the blood levels of ^{201}Tl. The redistribution of ^{201}Tl in a given myocardial region depends not only on the severity of the initial defect poststress but also on the presence of viable myocytes, the concentration of the tracer in the blood, and the rate of decline of ^{201}Tl levels in the blood (Fig. 4.14). During the redistribution phase, there is continuous exchange of ^{201}Tl between the myocardium and the extracardiac compartments, which is driven by the concentration gradient of the radiotracer across the myocytes, as well as blood and myocyte viability.

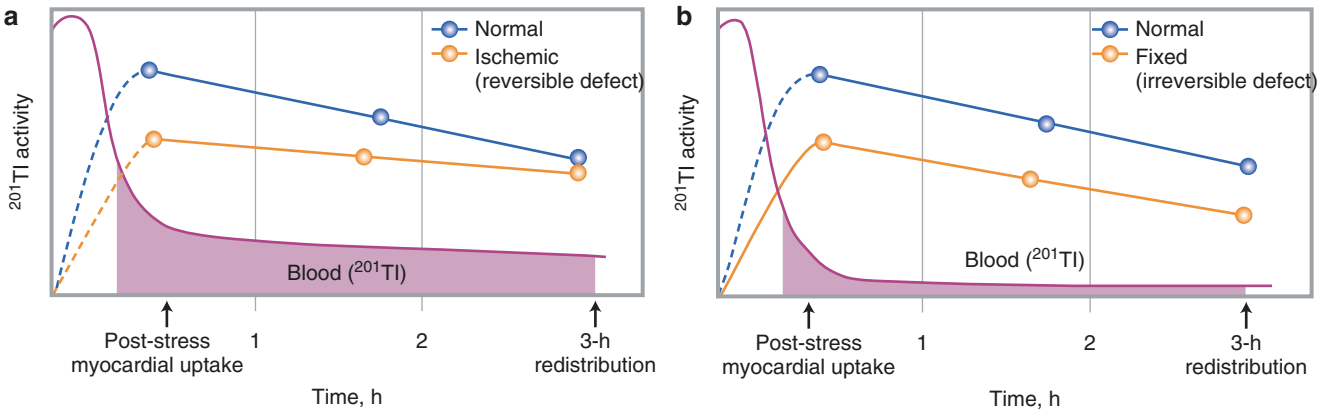

Fig. 4.14 Myocardial thallium uptake and clearance in relation to blood activity of thallium. (**a**) If the blood level of ^{201}Tl remains the same (or increases) during the period between stress and redistribution imaging, then a stress-induced defect in a region with viable myocytes that can accumulate ^{201}Tl in the redistribution phase will appear to be reversible. (**b**) If the blood level of ^{201}Tl is low (or decreases) during the imaging interval, the delivery of ^{201}Tl may be insufficient and the stress-induced ^{201}Tl defect may remain irreversible even though the underlying myocardium is viable. Thus, some ischemic but viable regions may show no redistribution on either early (3- to 4-hour) or late (24-hour) imaging, unless blood levels of ^{201}Tl are increased [19]

^{201}Tl reinjection (Fig. 4.15) differentiates ischemic but viable myocardium from scarred myocardium by augmenting the blood levels of ^{201}Tl at rest. A viable segment may be asynergic on the basis of repetitive stunning and hibernation. Thus, an asynergic but viable region may have reduced (but not absent) blood flow at rest (hibernation) or transient reduction in blood flow after a period of ischemia (stunning). Although standard stress 3- to 4-hour redistribution ^{201}Tl scintigraphy may underestimate the presence of ischemic but viable myocardium in many patients with coronary artery disease, reinjecting ^{201}Tl at rest after stress 3- to 4-hour redistribution imaging substantially improves the assessment of myocardial ischemia and viability in up to 49% of patients with apparently irreversible defects [2]. The theory that myocardial regions identified by ^{201}Tl uptake following ^{201}Tl reinjection represent viable myocardium is supported by improved regional function after revascularization and preserved metabolic activity by [^{18}F]-fluorodeoxyglucose PET. In addition, a significant inverse correlation between the magnitude of ^{201}Tl activity after reinjection and the regional volume fraction of interstitial fibrosis has been demonstrated in comparative clinicopathologic studies [20]. It is possible that the initial myocardial uptake of ^{201}Tl (postinjection) reflects regional blood flow, whereas the redistribution of ^{201}Tl in a given defect depends not only on the severity of the initial defect but also on the presence of viable myocytes, the concentration of the tracer in the blood, and the rate of decline of ^{201}Tl levels in the blood. Thus, the heterogeneity of regional blood flow observed in the initial stress-induced ^{201}Tl defects may be independent of the subsequent extent of ^{201}Tl redistribution. If the blood level of ^{201}Tl remains the same (or increases) during the period between stress and 3- to 4-hour redistribution imaging, then an apparent defect in a region with viable myocytes that can retain ^{201}Tl should improve. On the other hand, if the serum ^{201}Tl concentration decreases during the imaging interval, the delivery of ^{201}Tl may be insufficient, and the ^{201}Tl defect may remain irreversible although the underlying myocardium is viable. This suggests that some ischemic but viable regions may never redistribute, even with late (24-hour) imaging, unless serum levels of ^{201}Tl are increased. This hypothesis is supported by a study in which ^{201}Tl reinjection was performed immediately after 24-hour redistribution images were obtained [6]. Improved ^{201}Tl uptake after reinjection occurred in 40% of defects that appeared irreversible on late (24-hour) redistribution images. Thus, the reinjection of 1 mCi of ^{201}Tl at rest significantly improves the assessment of myocardial ischemia and viability.

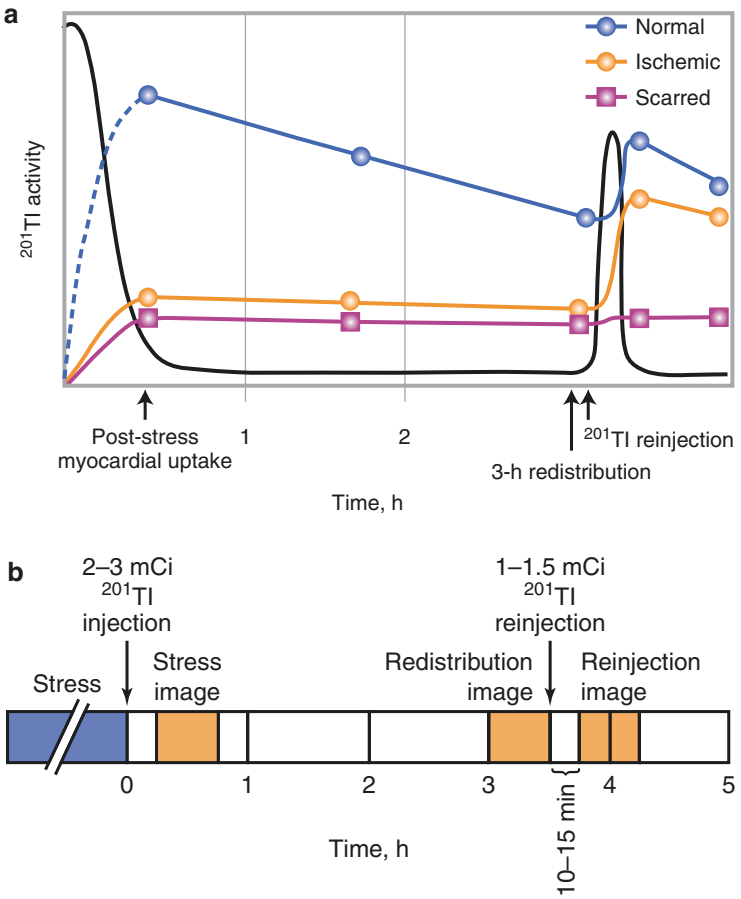

Fig. 4.15 Thallium reinjection. ^{201}Tl reinjection differentiates ischemic but viable myocardium from scarred myocardium by augmenting the blood levels of ^{201}Tl at rest. Reinjecting ^{201}Tl at rest after stress 3- to 4-hour redistribution imaging substantially improves the assessment of myocardial ischemia and viability in up to 49% of patients with apparently irreversible defects (**a**). If the blood level of ^{201}Tl remains the same (or increases) during the period between stress and 3- to 4-hour redistribution imaging, then an apparent defect in a region with viable myocytes that can retain ^{201}Tl should improve. On the other hand, if the serum ^{201}Tl concentration decreases during the imaging interval, the delivery of ^{201}Tl may be insufficient, and the ^{201}Tl defect may remain irreversible although the underlying myocardium is viable. This suggests that some ischemic but viable regions may never redistribute, even with late (24-hour) imaging, unless serum levels of ^{201}Tl are increased. Thus, the reinjection of 1 mCi of ^{201}Tl at rest immediately after either stress 3- to 4-hour redistribution (**b**) or stress 24-hour redistribution studies, followed by image acquisition 10–15 minutes later, significantly improves the assessment of myocardial ischemia and viability. (From Dilsizian [19]; with permission from Futura)

Figure 4.16 illustrates the beneficial effect of ^{201}Tl reinjection in the clinical setting. Among patients who had coronary artery revascularization, 87% of the myocardial regions identified as viable by reinjection studies had normal ^{201}Tl uptake and improved regional wall motion after revascularization. In contrast, all regions with irreversible defects in reinjection imaging before revascularization had persistent wall motion abnormality after revascularization [2]. Similar results were obtained when ^{201}Tl reinjection was performed immediately after late (24-hour) redistribution imaging. Improved ^{201}Tl uptake after reinjection occurred in 40% of regions (involving 60% of patients) that appeared to be fixed in late redistribution imaging [21].

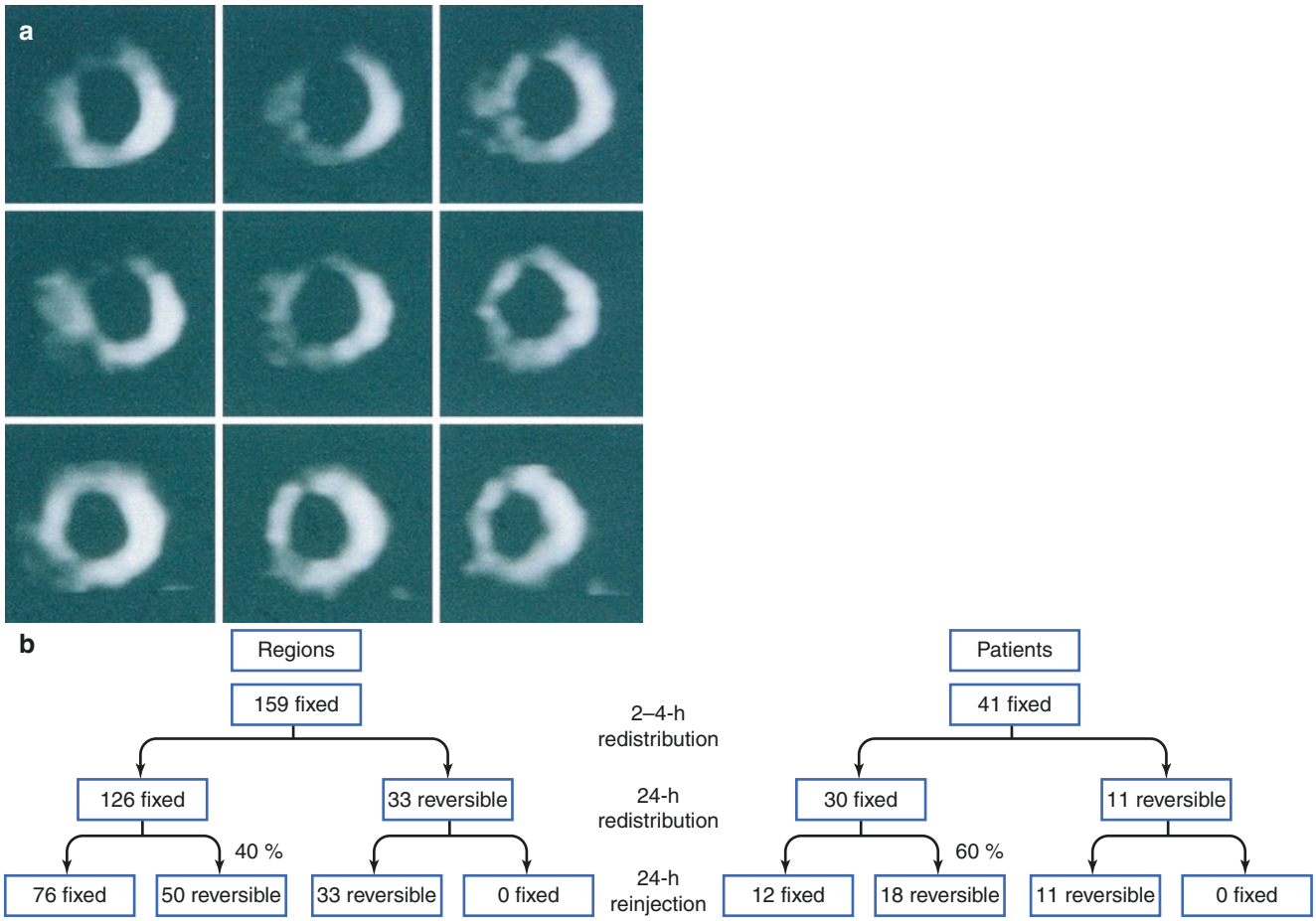

Fig. 4.16 Beneficial effect of ^{201}Tl reinjection in the clinical setting. (**a**) Short-axis tomograms demonstrate extensive ^{201}Tl defects in the anterior and septal regions in stress images (*top row*) that persist in redistribution images (*center row*) but improve markedly in reinjection images (*bottom row*) [2]. (**b**) Similar results were obtained when ^{201}Tl reinjection was performed immediately after late (24-hour) redistribution imaging. Improved ^{201}Tl uptake after reinjection occurred in 40% of regions (involving 60% of patients) that appeared to be fixed in late redistribution imaging [21]

Figure 4.17 shows the postrevascularization functional outcome of asynergic regions in relation to prerevascularization ^{201}Tl patterns of normal, reversible, partially reversible, mild-to-moderate irreversible, and severe irreversible defects using the stress-redistribution-reinjection ^{201}Tl protocol. The probabilities of functional recovery after revascularization were over 90% in normal or completely reversible defects, 63% in partially reversible defects, 30% in mild-to-moderate irreversible defects, but 0% in severe irreversible defects. Of asynergic regions with reversible defects (complete or partial) in the prerevascularization ^{201}Tl study, 79% had improved function after revascularization, but of asynergic regions with mild-to-moderate irreversible defects, only 30% had improved function ($P < 0.001$). Even at a similar mass of viable myocardial tissue (as reflected by the final ^{201}Tl content), the presence of inducible ischemia (reversible defect) was associated with an increased likelihood of functional recovery.

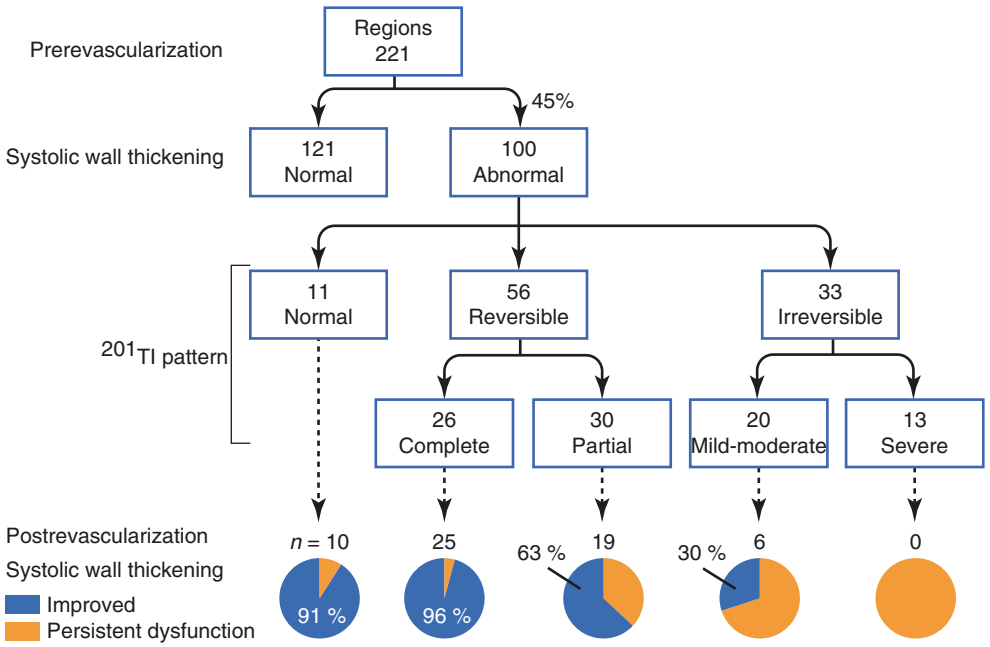

Fig. 4.17 Postrevascularization functional outcome of asynergic regions in relation to prerevascularization ^{201}Tl patterns [22]

In patients with prior myocardial infarction and left ventricular dysfunction in whom the assessment of myocardial viability is of clinical relevance, ^{201}Tl reinjection imaging provides incremental prognostic information to clinical, exercise tolerance testing, and ^{201}Tl stress-redistribution imaging (Fig. 4.18). Similarly, in patients with chronic coronary artery disease and prior myocardial infarction, the scintigraphic variable that was the strongest predictor of hard events (cardiac death or myocardial infarction) was the presence of more than three irreversible defects that remained irreversible after ^{201}Tl reinjection.

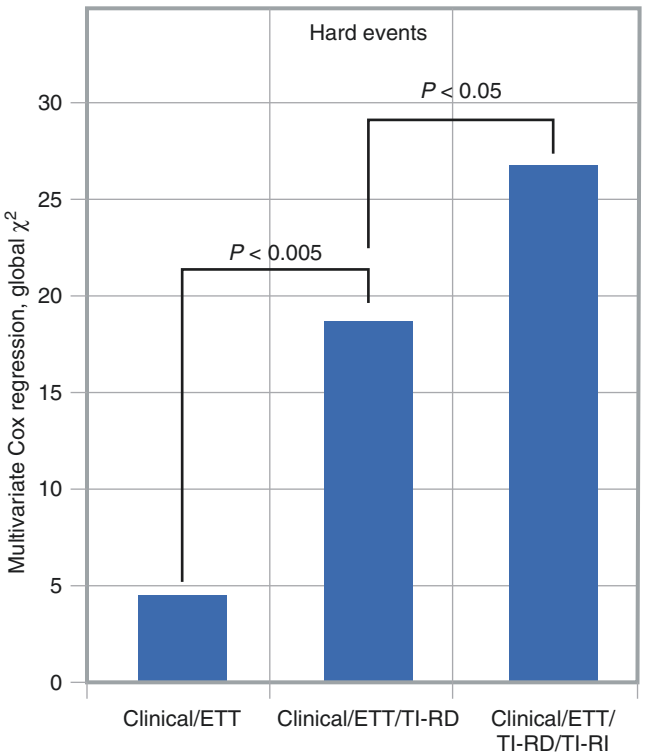

Fig. 4.18 Incremental prognostic value of ^{201}Tl reinjection (Tl-RI). Tl-RD—^{201}Tl stress-redistribution imaging [23]

The stress-redistribution-reinjection ^{201}Tl protocol provides important diagnostic information regarding both inducible ischemia and myocardial viability. In most cases, the identification of myocardial ischemia is much more important clinically in terms of patient management and risk stratification than is knowledge of myocardial viability. But if the clinical question is one of the presence and extent of viable myocardium within a dysfunctional region, not inducible ischemia, then it is reasonable to perform rest-redistribution ^{201}Tl imaging only (Fig. 4.19). Finding significant reversibility is suggestive of hibernating but viable myocardium [24].

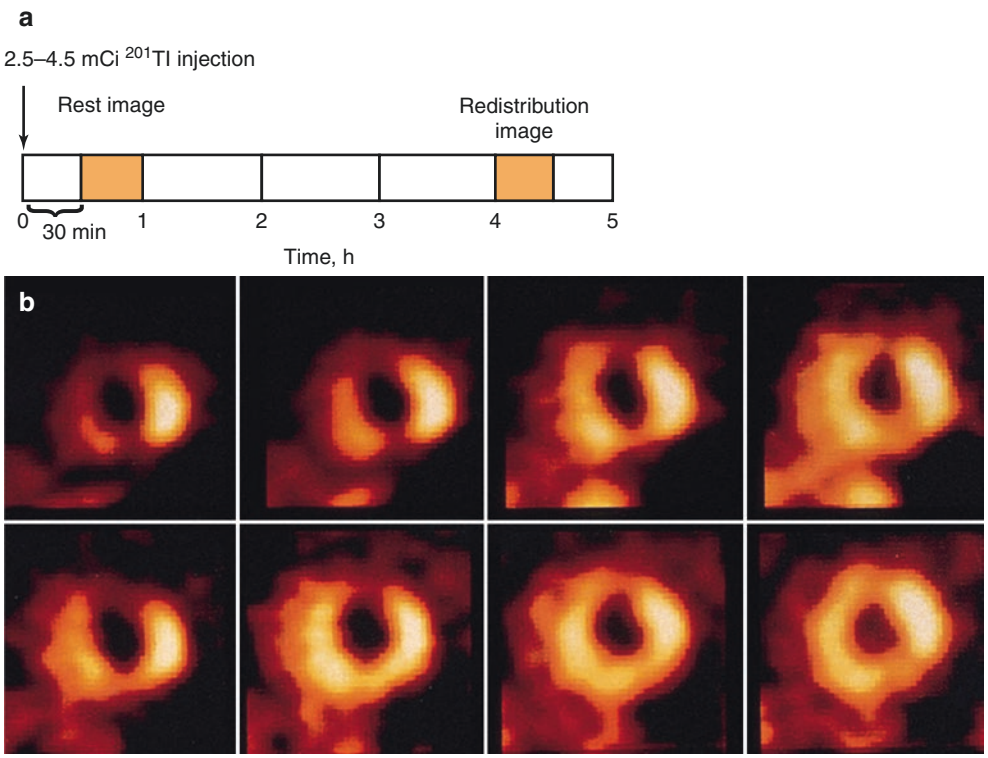

Fig. 4.19 (**a**) Rest-redistribution ^{201}Tl protocol. (**b**) Rest-redistribution short-axis ^{201}Tl tomograms are shown for a patient with chronic coronary artery disease. There are extensive ^{201}Tl perfusion defects in the anterior, distal anteroseptal, and inferior regions in the initial rest images (*top row*). In the delayed (3- to 4-hour) redistribution images (*bottom row*), the anterior region remains fixed (scarred myocardium), but the inferior and distal anteroseptal regions show significant reversibility, which is suggestive of hibernating but viable myocardium [24]

Accurate distinction between viable (hibernating or stunned) and scarred myocardium has important clinical implications. Ideally, such information may be used to guide therapeutic decisions for revascularization and risk stratification. Anatomic assessment of the coronary arteries alone does not differentiate viable from scarred myocardium, as illustrated in Fig. 4.20. The anatomic assessment of this patient's coronary arteries alone was insufficient to determine whether the myocardium subtended by the totally occluded vessels was viable or scarred. The scintigraphic finding of reduced regional blood flow (rest ^{201}Tl images) but preserved cell membrane integrity (redistribution ^{201}Tl images) in the dysfunctional myocardial regions provided the most direct evidence of myocardial hibernation. In view of the findings on the rest-redistribution ^{201}Tl study, the patient was referred for coronary artery bypass surgery with an uneventful postoperative course.

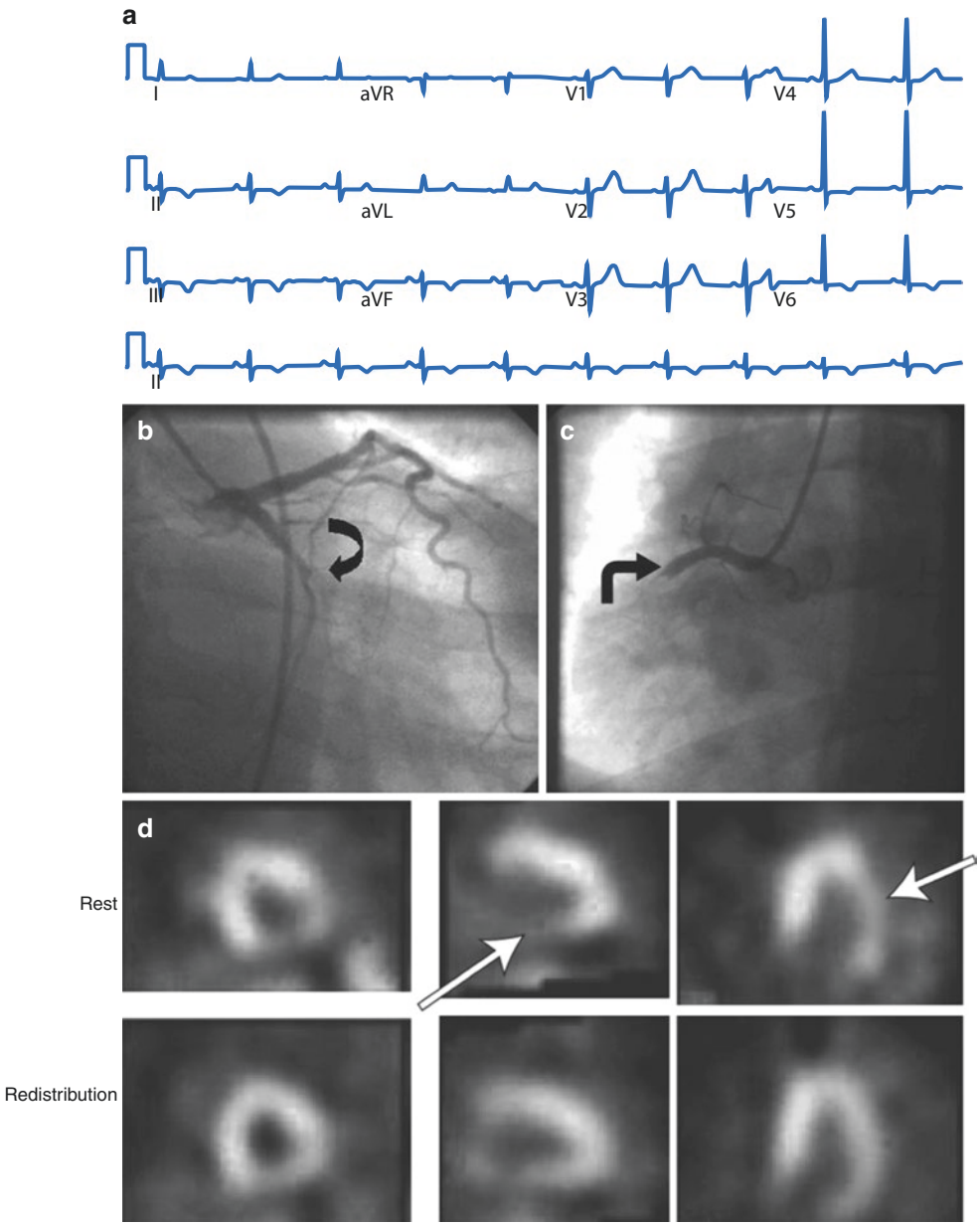

Fig. 4.20 Using a rest-redistribution ^{201}Tl study to differentiate viable from scarred myocardium. A patient with a prior history of hypertension and hyperlipidemia presents with a 2-month history of substernal chest pain. The electrocardiogram shows inverted T waves in the inferolateral leads (**a**); the coronary angiogram shows total occlusion of the left circumflex (LCX) (*arrow*) (**b**) and the proximal right coronary artery (RCA) (*arrow*) (**c**). Extensive perfusion defects in the lateral and inferior regions (**d**) in the initial rest images (*top row*; *arrows*) become reversible in the delayed (3- to 4-hour) redistribution images (*bottom row*), providing evidence for hypoperfused but viable myocardium in the LCX and RCA vascular territories. In view of the findings on the rest-redistribution ^{201}Tl study, the patient was referred for coronary artery bypass surgery with an uneventful postoperative course

Figure 4.21 demonstrates the prognostic value of rest-redistribution ^{201}Tl SPECT. In patients with chronic ischemic left ventricular dysfunction, the demonstration of redistribution on rest ^{201}Tl imaging protocols portends a higher mortality rate with medical therapy than the rate for patients with a comparable degree of left ventricular dysfunction without evidence of redistribution.

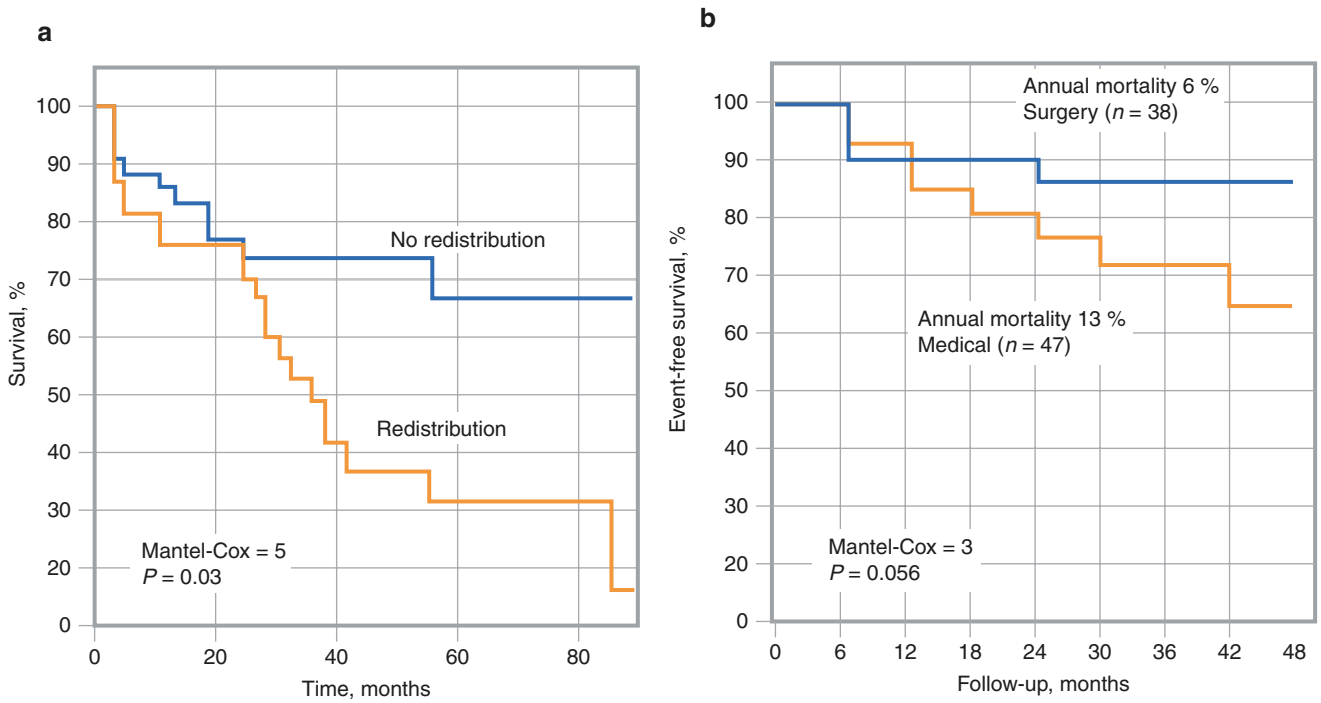

Fig. 4.21 Prognostic value of rest-redistribution ^{201}Tl SPECT. (**a**) An actuarial survival curve in 81 medically treated patients is shown; 38 patients with a mean left ventricular ejection fraction (LVEF) of 26 ± 7% showed redistribution in rest ^{201}Tl images, and 43 patients (mean LVEF, 27 ± 8%) showed no redistribution. Moreover, in a nonrandomized, retrospective study with rest-redistribution ^{201}Tl, survival and survival without myocardial infarction tended to be significantly higher in patients with chronic ischemic left ventricular dysfunction treated with coronary artery revascularization, compared with those treated with medical therapy alone. (**b**) An actuarial survival curve in 85 patients with evidence of myocardial viability by rest-redistribution ^{201}Tl is shown; 38 patients underwent coronary artery revascularization, and 47 patients were treated medically [25, 26]

Considering the survival advantage of coronary artery revascularization when compared with medical therapy in patients with chronic ischemic left ventricular dysfunction, one might question whether the preoperative assessment of myocardial viability is necessary in making revascularization decisions. Should coronary artery revascularization be considered in all patients with chronic ischemic left ventricular dysfunction, with or without evidence of myocardial viability? Figure 4.22 shows event-free survival in a retrospective study in patients with preoperative rest-redistribution ^{201}Tl testing, all of whom had coronary artery bypass surgery. Perioperative and long-term postoperative survival was significantly better in the patients with evidence of significant myocardial viability on rest-redistribution ^{201}Tl than in those with less evidence of myocardial viability.

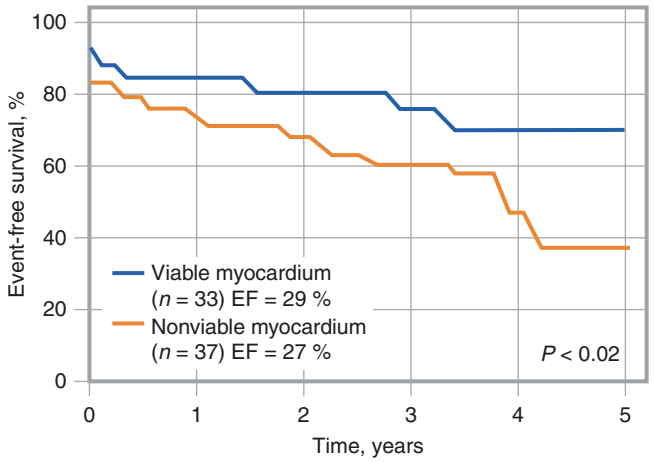

Fig. 4.22 Patient outcome (event-free survival) after coronary artery bypass surgery in patients with more or less viable myocardium as assessed by rest-redistribution ^{201}Tl and ejection fraction (EF) [27]

Table 4.4 lists the features of SPECT techniques using ^{201}Tl. The myocardial extraction of ^{201}Tl is dependent on energy utilization, membrane ATPase, and active transport. ^{201}Tl does not actively concentrate in regions of infarcted or scarred myocardium, so decreased myocardial ^{201}Tl uptake early after injection can be caused either by reduced regional blood flow or by infarction. Experimental studies with ^{201}Tl have shown that the cellular extraction of ^{201}Tl across the cell membrane is unaffected by hypoxia unless an irreversible injury is present. Similarly, pathophysiologic conditions of chronic hypoperfusion (hibernation) and postischemic dysfunction (stunning), in which regional contractile function is impaired in the presence of myocardial viability, do not adversely alter the extraction of ^{201}Tl.

Monovalent cation with biologic properties similar to potassium
60–80 keV mercury x-ray emission, 73-hour physical half-life
High first-pass extraction fraction (~85%)
Transported across myocyte sarcolemmal membrane via the Na–K ATPase transport system and by facilitative diffusion
Peak myocardial concentration within 5 minutes of intravenous injection
Rapid clearance from the intravascular compartment
Redistribution begins 10–15 minutes after injection

Table 4.4 SPECT techniques: ^{201}Tl

SPECT Techniques: ^{99m}Tc-labeled Perfusion Tracers

Alternatively, dual-isotope gated SPECT can be performed (Fig. 4.23); this technique combines rest-redistribution ^{201}Tl (for viability) with stress ^{99m}Tc-sestamibi or ^{99m}Tc-tetrofosmin (for perfusion), thereby taking advantage of the favorable properties of each of the two tracers.

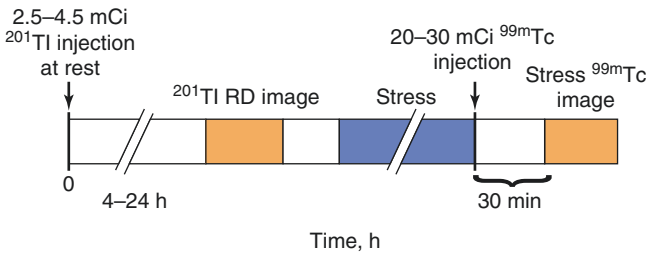

Fig. 4.23 Dual-isotope gated SPECT protocol, combining rest-redistribution ^{201}Tl (for viability) with stress ^{99m}Tc-sestamibi or ^{99m}Tc-tetrofosmin (for perfusion). RD—redistribution

Figures 4.24, 4.25, and 4.26 illustrate the differences between ^{201}Tl and ^{99m}Tc-sestamibi in various studies in animals and humans.

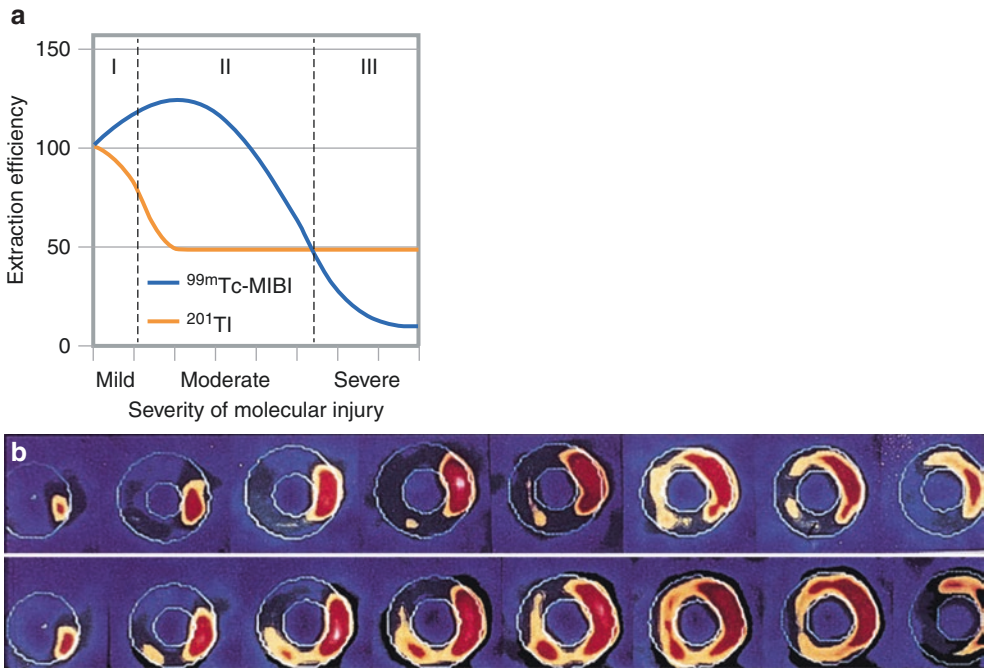

Fig. 4.24 Cellular kinetics of ^{201}Tl and ^{99m}Tc-sestamibi during metabolic inhibition in cultured chick embryo cardiac myocytes, independent of perfusion. (**a**) Oxidative phosphorylation and glycolysis were inhibited simultaneously by rotenone (10 μM) and iodoacetate (1 mmol/L), respectively, producing a decline in the myocellular ATP content. Under these conditions, the initial extraction efficiency of ^{201}Tl and ^{99m}Tc-sestamibi responded in divergent ways to ATP depletion. The extraction efficiency of ^{201}Tl declined within 20 minutes of metabolic inhibition by 50–70%, whereas the extraction efficiency of ^{99m}Tc-sestamibi (^{99m}Tc-MIBI) increased significantly within 10–20 minutes and remained elevated for the first 40–60 minutes of metabolic inhibition. The observed disparity in initial uptake rates between ^{201}Tl and ^{99m}Tc-MIBI during mild to moderate metabolic injury may explain, on a metabolic basis alone, the clinical observation that ^{99m}Tc-MIBI defects are smaller than those assessed by ^{201}Tl [28]. (**b**) Images taken with ^{201}Tl 5–10 minutes after stress (*top row*) and with ^{99m}Tc-MIBI 2 hours after stress (*bottom row*) are shown for a patient who performed the same level of exercise with both tracers. A quantitative left ventricular mass algorithm provided similar measures of total mass for ^{201}Tl (197 g) and for ^{99m}Tc-MIBI (189 g), but the stress-induced defect mass derived from ^{201}Tl imaging (41 g) is significantly larger than that detected by ^{99m}Tc-MIBI (30 g). No transmural defects are present on the ^{99m}Tc-MIBI images. (*From* Narahara et al. [29], with permission from Elsevier)

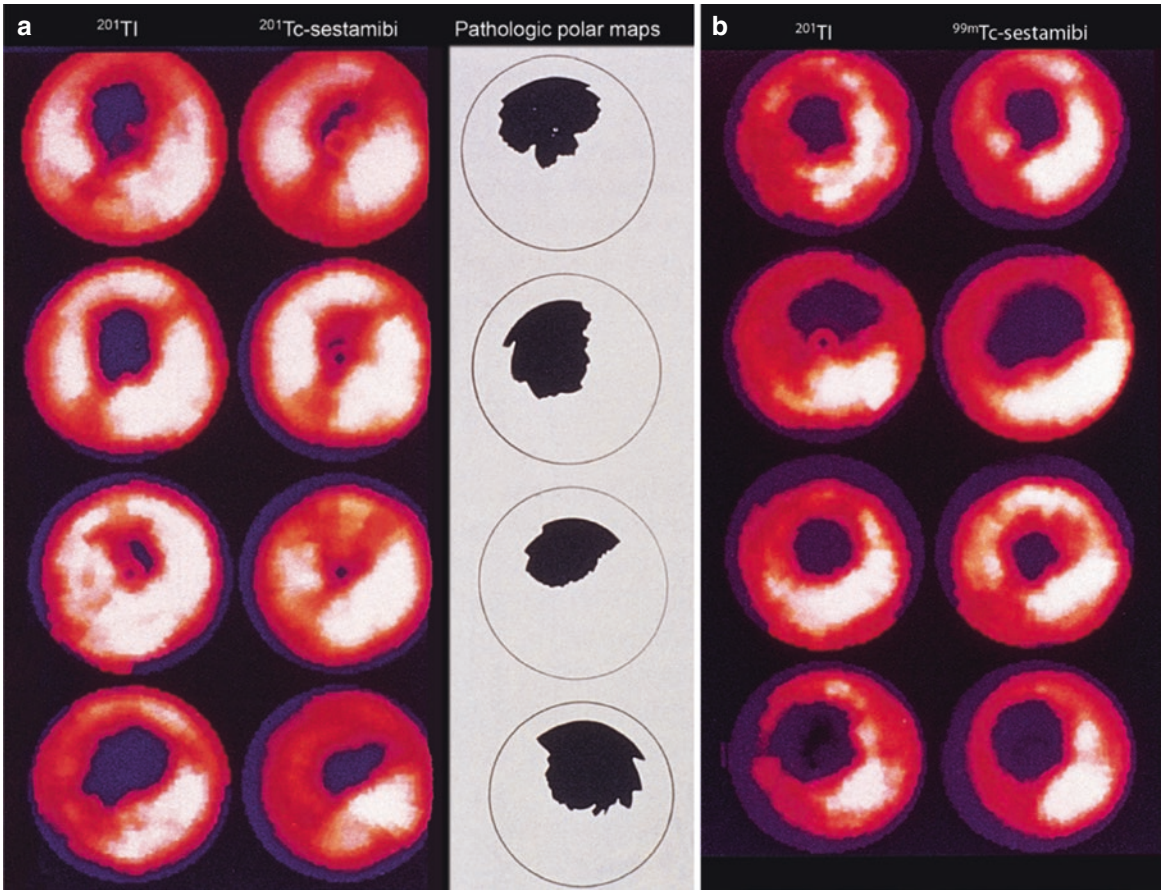

Fig. 4.25 Pharmacologic stress. In canine models of moderate (**a**) and severe (**b**) coronary artery occlusion, ^{201}Tl and ^{99m}Tc-sestamibi myocardial perfusion defect sizes are compared during pharmacologic stimulation and with postmortem staining to define the extent of the hypoperfused region. These bull's-eye displays are from four representative experiments of moderate coronary artery stenosis during pharmacologic stimulation for ^{201}Tl and ^{99m}Tc-sestamibi, and the corresponding pathologic polar displays from the same four experiments are shown. The extent of ^{201}Tl myocardial perfusion defect size (but not ^{99m}Tc-sestamibi) approaches the hypoperfused area in the corresponding pathologic display. The ^{99m}Tc-sestamibi defect size occupies only 37% of the area of the defect in the ^{201}Tl images of the same dog, and the counts within the defects are 39% higher for ^{99m}Tc-sestamibi compared with ^{201}Tl (**a**). On the other hand, when coronary artery occlusion is near total (severe), ^{201}Tl and ^{99m}Tc-sestamibi show similar defect contrast and areas (**b**). These observations in canines are similar to the experimental observations made in cultured myocytes. (*From* Leon et al. [30], with permission from Elsevier)

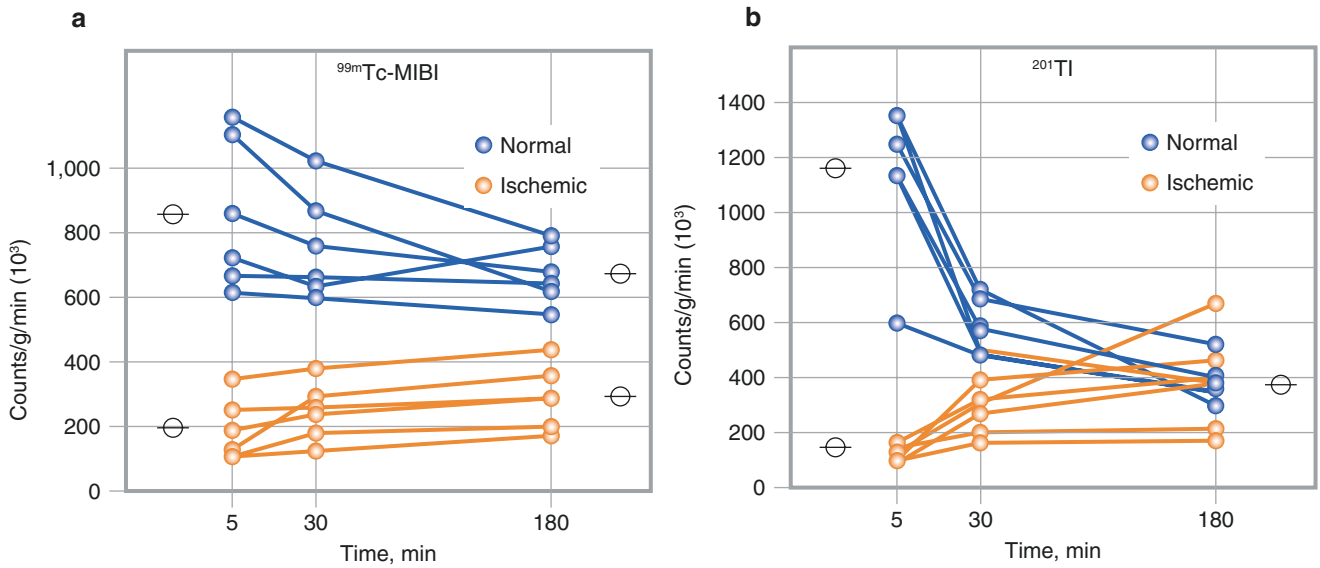

Fig. 4.26 ^{99m}Tc-sestamibi and ^{201}Tl activities in myocardial biopsies. A change in defect size of ^{99m}Tc-sestamibi (^{99m}Tc-MIBI) with time (redistribution) has been shown both in animal models and in patients with chronic coronary artery disease [31, 32]. Depending on the level of blood activity of ^{99m}Tc-MIBI after stress, continued uptake by the myocardium after the first pass may reduce the defect severity and area in the hypoperfused region. In the early comparative studies of ^{201}Tl and ^{99m}Tc-MIBI, ^{201}Tl images were acquired 5–10 minutes after injection, and the ^{99m}Tc-MIBI images were acquired 1–2 hours after injection. The 1- to 2-hour delay between ^{99m}Tc-MIBI injection and imaging was based on the best compromise between a high myocardial count rate and low background activity, and on the assumption that ^{99m}Tc-MIBI does not "redistribute" over time. Following transient ischemia and reperfusion after 5 minutes in a canine model, there was evidence for change in the defect size of ^{99m}Tc-MIBI with time (**a**), albeit more slowly and less completely than the ^{201}Tl redistribution (**b**). For both ^{99m}Tc-MIBI and ^{201}Tl, a consistent fall in the normal zone activity and rise in the ischemic zone activity are noted over the 3-hour time interval, which is consistent with redistribution. It is important to point out, however, that there is no change in the ^{99m}Tc-MIBI defect size between the 5-minute and 30-minute time intervals. In view of these and other similar reports, it is now recommended that ^{99m}Tc-MIBI images be acquired earlier, approximately 30 minutes after injection of the tracer [31]

Figure 4.27 illustrates clinically relevant change in the defect size of ^{99m}Tc-sestamibi with time (redistribution). Interpretation of ^{99m}Tc-sestamibi data should be viewed cautiously when imaging is delayed by 2 hours or more after stress (due to underestimation of the defect size and extent of myocardial ischemia), but the same concept does not apply for rest-injected ^{99m}Tc-sestamibi studies. On the contrary, delaying ^{99m}Tc-sestamibi images by 2 hours or more after rest injection may improve myocardial viability assessment.

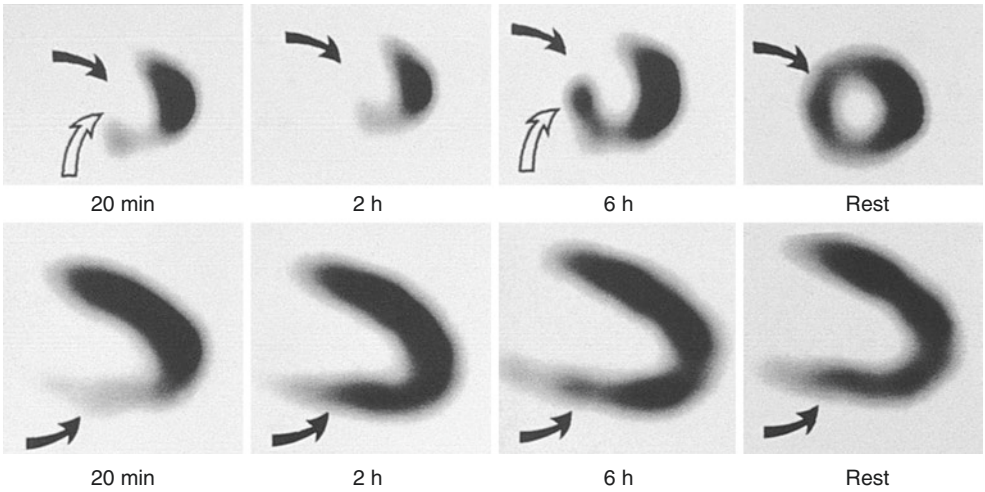

Fig. 4.27 Clinically relevant change in the defect size of ^{99m}Tc-sestamibi with time (redistribution) in two patients who experienced exercise ^{99m}Tc-sestamibi studies. Myocardial SPECT images obtained from two different patients are presented in the short-axis plane (*top row*) and in the vertical long-axis plane (*bottom row*) after exercise and at rest. In the short-axis plane, there is no change in ^{99m}Tc-sestamibi defect size from 20 minutes to 2 hours after exercise, but by 6 hours there is a significant change in the defect size in the inferoseptal region (*open arrow*) but not in the anteroseptal region (*closed arrow*). In the injected image taken at rest, complete normalization of all perfusion defects is seen, which suggests that delayed ^{99m}Tc-sestamibi images alone do not provide accurate information regarding defect reversibility. In the vertical long-axis plane, there is significant change in the ^{99m}Tc-sestamibi defect in the inferior region (*closed arrows*) from 20 minutes to 2 hours after exercise (redistribution), without further fill-in at 6 hours or in the rest-injected ^{99m}Tc-sestamibi image [33]

Considering the kinetics of ^{99m}Tc-sestamibi and ^{99m}Tc-tetrofosmin, uptake of these radiotracers in myocardial regions with reduced perfusion and partially impaired viability appears to be influenced by regional perfusion rather than myocyte viability. In view of the limitations in the clinical setting of rest-injected ^{99m}Tc-sestamibi and ^{99m}Tc-tetrofosmin for assessing myocardial viability, some investigators have proposed injecting the radiotracers during nitrate infusion. In addition to lowering the preload and afterload, nitrates may cause vasodilatation of the flow, limiting epicardial coronary arteries as well as collateral vessels. The injection of ^{99m}Tc-sestamibi during nitrate infusion (10 mg of isosorbide dinitrate in 100 mL of isotonic saline solution infused over 20 minutes) is shown to improve the accuracy of ^{99m}Tc-sestamibi for predicting the recovery of regional and global left ventricular function after revascularization. Figure 4.28 shows an example of a patient with anterior myocardial infarction and single-vessel left anterior descending (LAD) coronary artery disease [34].

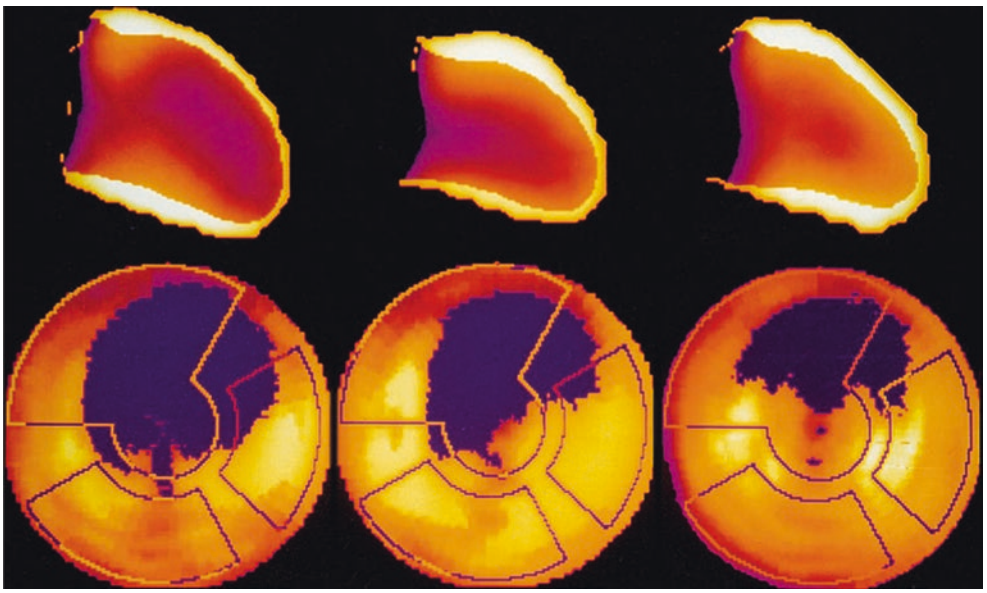

Fig. 4.28 Nitrate administration before rest ^{99m}Tc-sestamibi or ^{99m}Tc-tetrofosmin injection. In this example of a patient with anterior myocardial infarction and single-vessel left anterior descending (LAD) coronary artery disease, the prerevascularization baseline images (*left*) show anteroapical akinesis and global left ventricular ejection fraction (LVEF) of 38% in first-pass radionuclide angiography, associated with a large anterior and apical ^{99m}Tc-sestamibi perfusion defect (63% of the LAD vascular territory in the bull's-eye image at rest). The ^{99m}Tc-sestamibi images acquired after nitrate infusion (*center*) show improvement in the anteroapical wall motion associated with an increase in global LVEF to 42% and a decrease in the extent of ^{99m}Tc-sestamibi perfusion defect size to 42% of the LAD vascular territory. After revascularization of the LAD (*right*), there is improvement in the anteroapical wall motion at rest, an increase in global LVEF to 45%, and a decrease in the extent of ^{99m}Tc-sestamibi perfusion defect to 38% of the LAD vascular territory [34]. (*Courtesy of* Roberto Sciagra)

Another approach that may overcome, in part, the limitations of ^{99m}Tc-sestamibi and ^{99m}Tc-tetrofosmin in assessing myocardial viability is to quantify the severity of regional tracer activity, i.e., the severity of myocardial perfusion at rest. Figure 4.29 demonstrates a good correlation between the quantitative regional activities of ^{201}Tl (on redistribution imaging after rest injection) and ^{99m}Tc-sestamibi (at rest). In addition, dysfunctional myocardial regions that improve function after revascularization can be differentiated from dysfunctional myocardial regions that do not improve function after revascularization. In myocardial regions with decreased blood flow and partially impaired viability, the uptake of ^{99m}Tc-sestamibi appears to be influenced by regional perfusion rather than myocyte viability [35].

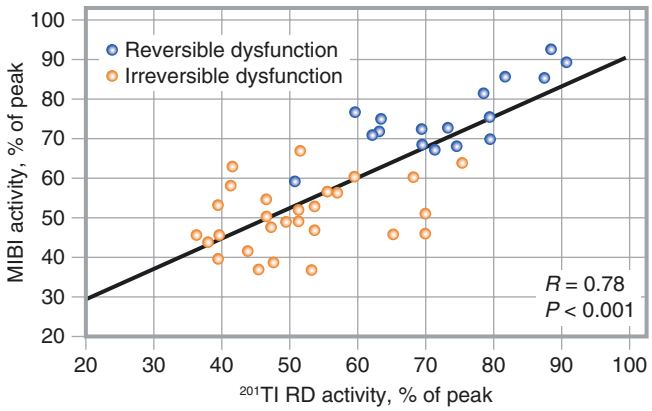

Fig. 4.29 Quantitation of severity of reduction in myocardial perfusion at rest. Among 18 patients with coronary artery disease who had revascularization, a good correlation between the quantitative regional activities of ^{201}Tl (on redistribution [RD] imaging after rest injection) and ^{99m}Tc-sestamibi (at rest) is shown. This scatterplot shows that at a 60% threshold level for both radiotracers, dysfunctional myocardial regions that improve function after revascularization (*blue circles*) can be differentiated from dysfunctional myocardial regions that do not improve function after revascularization (*orange circles*). When the severity of radiotracer defects were quantitated, the positive predictive accuracy was 80% and the negative accuracy was 96% [36]

A study comparing myocardial viability seen on rest ^{99m}Tc-sestamibi SPECT with metabolism assessed by [^{18}F]-fluorodeoxyglucose (FDG) show a mismatch, as seen in Fig. 4.30.

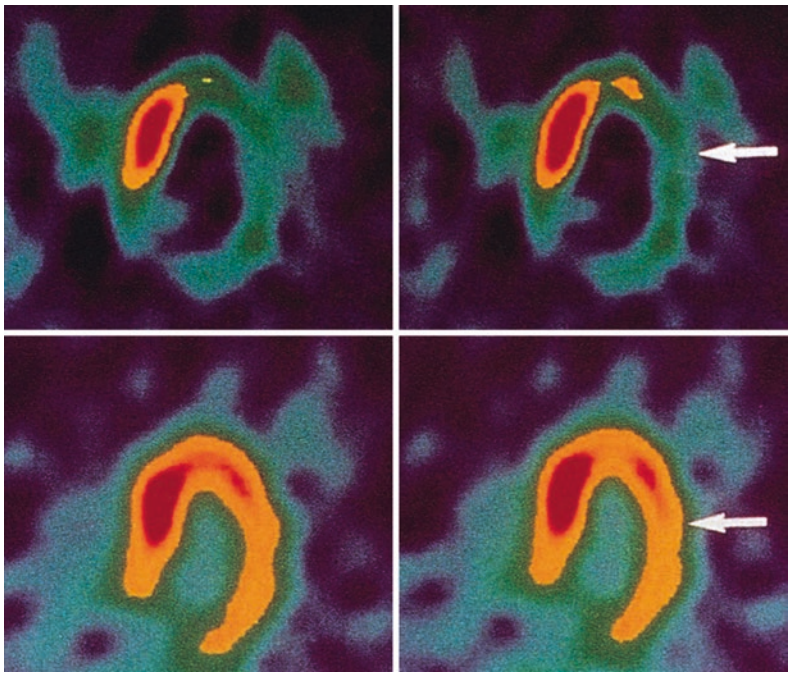

Fig. 4.30 Underestimation of myocardial viability by rest ^{99m}Tc-sestamibi SPECT. Using dual-isotope injection at rest (same physiologic state) and simultaneous acquisition using SPECT (accurate anatomical alignment), these images show mismatch between rest cardiac perfusion assessed by ^{99m}Tc-sestamibi and metabolism assessed by [^{18}F]-fluorodeoxyglucose (FDG). After oral glucose loading, the patient was injected with 10 mCi of FDG and 25 mCi of ^{99m}Tc-sestamibi at rest. Dual-isotope single acquisition SPECT was performed approximately 60 minutes later by positioning two 20% pulse-height analyzer windows symmetrically around the 140-keV photopeak of ^{99m}Tc and the 511-keV photopeak of FDG. The digital electronics of the camera permitted frame-by-frame decay correction for short-lived FDG. Thus, two separate sets of slices mapping the ^{99m}Tc-sestamibi and FDG distribution were simultaneously obtained, resulting in one-to-one correspondence in spatial registration. Rest ^{99m}Tc-sestamibi images in the horizontal long-axis plane (*top row*) show reduced perfusion in the apical and lateral regions (*arrow*). Corresponding FDG images (*bottom row*) show preserved metabolism in the apical and lateral regions, suggestive of viable myocardium (*arrow*) [37]

As listed on Table 4.5, ^{99m}Tc-sestamibi (isonitrile) and ^{99m}Tc-tetrofosmin are both lipophilic cationic complexes with similar myocardial uptake and blood clearance kinetics. However, the clearance of tetrofosmin from the lungs and the liver is faster than ^{99m}Tc-sestamibi, which may improve the resolution of cardiac images and reduce the overall radiation burden. Both ^{99m}Tc-sestamibi and ^{99m}Tc-tetrofosmin are taken up across the sarcolemmal and mitochondrial membranes of myocytes by passive distribution and are retained within the mitochondria at equilibrium, owing to a large negative transmembrane potential. Experimental studies with ^{99m}Tc-sestamibi have shown that myocardial uptake and clearance are related to the mitochondrial transmembrane potential and do not differ from ischemic to nonischemic regions. In addition, experimental studies of myocardial infarction, with and without reperfusion, have fueled optimism in the clinical use of ^{99m}Tc-sestamibi for myocardial viability assessment. In the clinical setting, however (with the exception of a few studies), both ^{99m}Tc-sestamibi and ^{99m}Tc-tetrofosmin appear to underestimate myocardial viability. Compared with ^{201}Tl and PET tracers, factors that may contribute to the impaired accumulation of ^{99m}Tc-sestamibi or ^{99m}Tc-tetrofosmin in viable regions at rest include differences in the extraction fraction, blood clearance, redistribution, and response to altered metabolic states. Perhaps a likely improvement in viability assessment could be achieved through nitrate administration before rest ^{99m}Tc-sestamibi injection and the quantitation of regional radiotracer uptake.

Lipid-soluble cationic compounds
140-keV photopeak energy, 6-hour physical half-life
First-pass extraction fraction ~60%
Uptake is passive across mitochondrial membranes
At equilibrium, retention within the mitochondria is due to a large negative transmembrane potential
Clearance from the intravascular compartment via hepatobiliary excretion
Minimal redistribution when compared with ^{201}Tl

Table 4.5 SPECT techniques: ^{99m}Tc-labeled Sestamibi and ^{99m}Tc-labeled Tetrofosmin

Table 4.6 lists the characteristics of another agent used in SPECT, ^{99m}Tc-teboroxime. ^{99m}Tc-teboroxime is a neutral, lipophilic BATO (boronic acid adducts of technetium dioxime) compound with a reported first-pass extraction of 88% at rest and 91% under hyperemic conditions. Unlike ^{99m}Tc-sestamibi and ^{99m}Tc-tetrofosmin, clearance of teboroxime from the myocardium is rapid and the washout rate is proportional to blood flow. In experimental studies, approximately two thirds of the teboroxime activity has been shown to clear from the heart, with a half-life of 3.6 minutes. Thus, both uptake and clearance of teboroxime from the myocardium are proportional to regional blood flow and are not confounded by tissue metabolism or other binding characteristics within the myocardium.

Neutral, lipophilic compound
140-keV photopeak energy, 6-hour physical half-life
High first-pass extraction fraction under hyperemic conditions (~91%)
Extraction by the myocardium remains linear even at high-flow conditions
Rapid clearance from the myocardium at a rate proportional to regional blood flow
Uptake and washout are independent of the metabolic status of the myocardial cells

Table 4.6 SPECT techniques: ^{99m}Tc-Teboroxime

PET Tracers and Techniques

Figure 4.31 shows examples of positron emission tomography (PET) myocardial perfusion images using rubidium-82 (^{82}Rb), which offer the potential for overlaying coronary anatomic information from hybrid PET/CT angiography. Gated ^{82}Rb PET images provide an indirect evaluation of abnormal myocardial perfusion as reflected in regional wall motion abnormalities during stress, as opposed to poststress with SPECT.

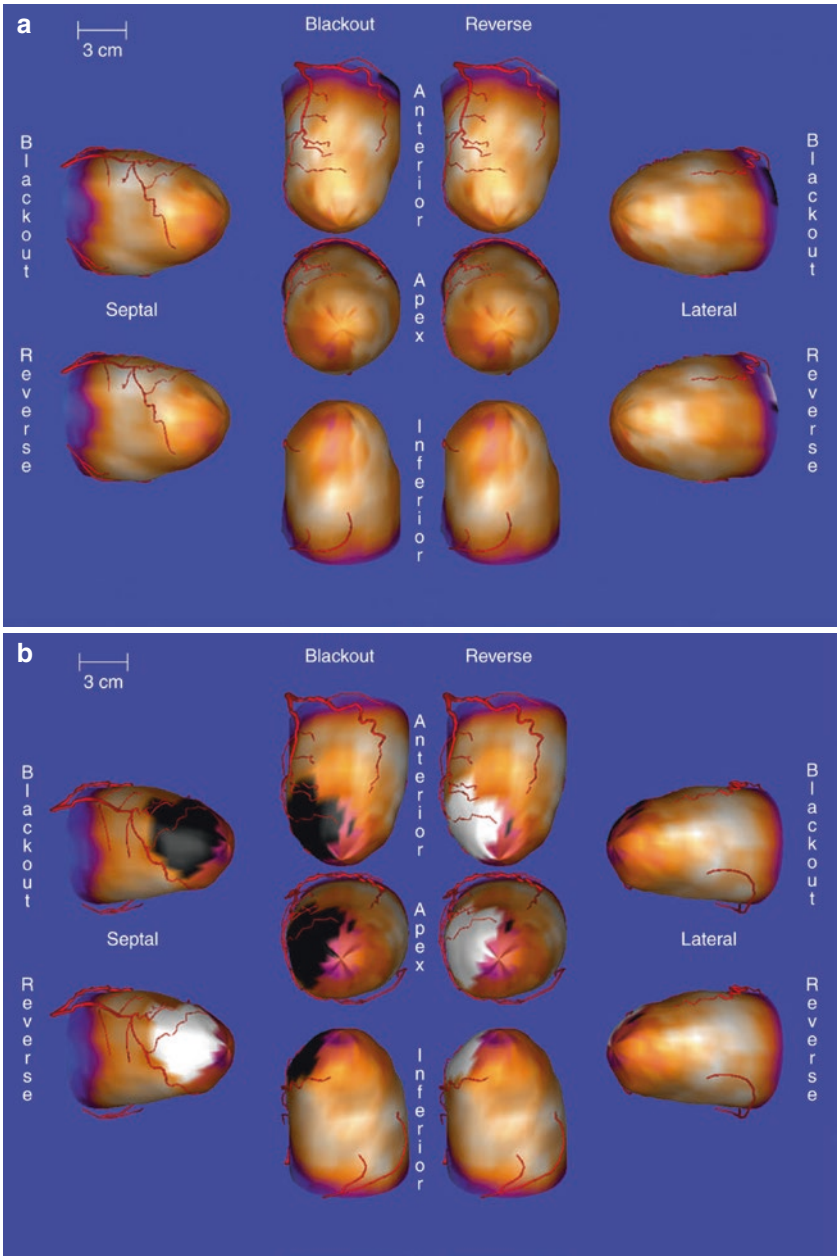

Fig. 4.31 Positron emission tomography (PET) techniques: rubidium-82 (^{82}Rb). Examples of three-dimensional (3D) surface-rendered models of normal (**a**) and abnormal (**b**) ^{82}Rb PET myocardial perfusion images are shown, with the potential for overlaying coronary anatomic information from hybrid PET/CT angiography. Although the first few minutes after the infusion of ^{82}Rb are not usually included in clinical acquisition protocols, it is precisely this period that is of interest if myocardial perfusion is to be quantified (**c**).

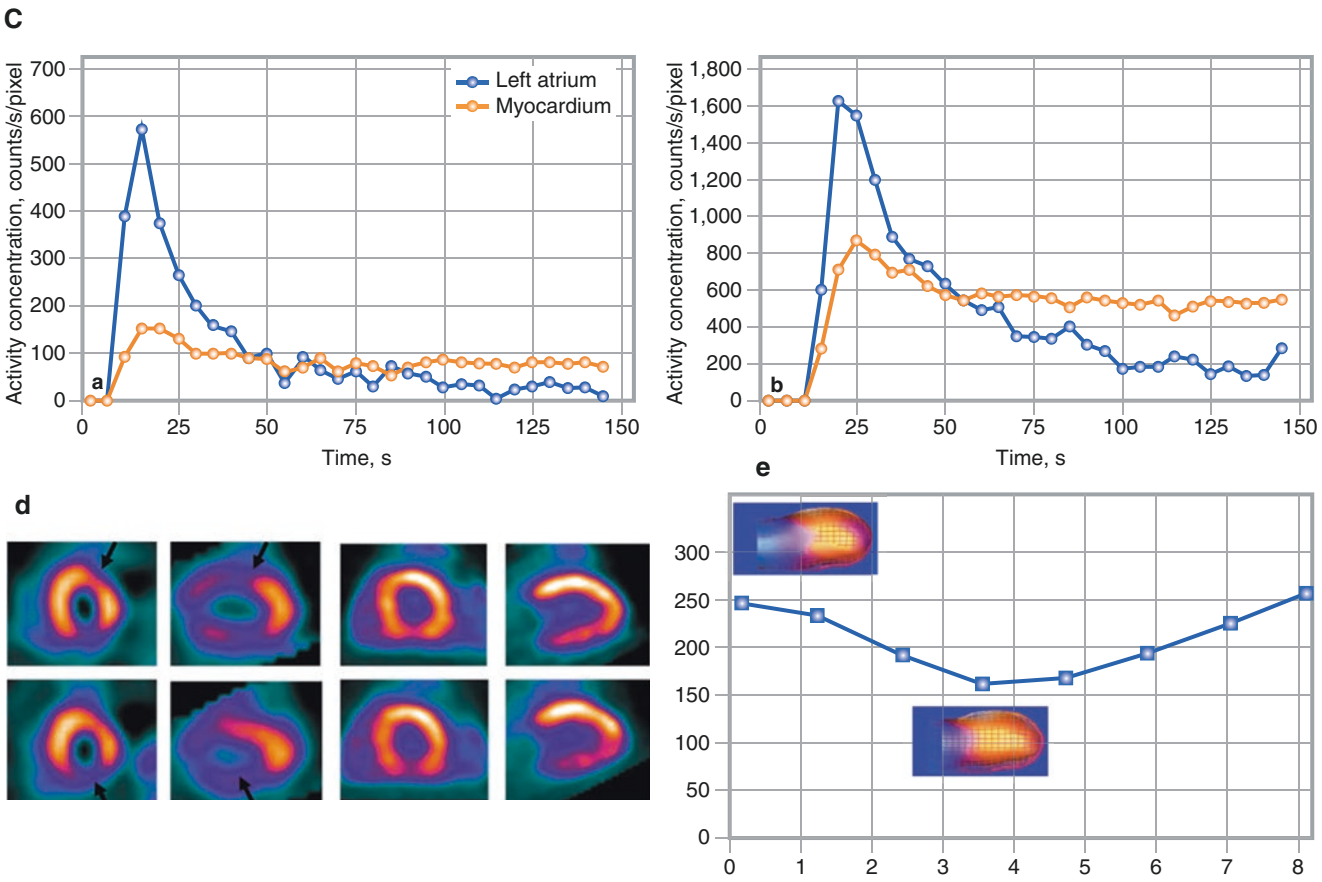

Fig. 4.31 (continued) Dynamic imaging of the heart during this time allows analysis of the ^{82}Rb concentration in both arterial blood and myocardial tissue as a function of time. ^{82}Rb time–activity curves are shown at rest (*left*) and after adenosine stress (*right*). The circles represent the activity concentration in the left atrium and in the myocardial tissue. The myocardial perfusion SPECT and ^{82}Rb PET studies show a disparity (**d**). Clinically indicated adenosine dual-isotope gated SPECT images (*left panel*) without attenuation correction show a regional ^{99m}Tc-sestamibi perfusion defect in the anterior and inferior regions (*arrows*). In the rest ^{201}Tl images, the anterior defect became reversible, but the inferior defect persisted. Corresponding ^{82}Rb PET myocardial perfusion tomograms performed in the same patient are shown in the *right panel*. PET images were acquired from a PET/CT scanner after an infusion of adenosine and 30 mCi of ^{82}Rb (*top*) and at rest following another 30-mCi infusion of ^{82}Rb (*bottom*). The ^{82}Rb PET images show normal distribution of the radiotracer in all myocardial regions, without evidence for a reversible or fixed defect to suggest myocardial ischemia or infarction. Although the high-energy positrons of ^{82}Rb degrade spatial resolution and the short half-life increases statistical noise, high-quality images free from attenuation artifacts can be produced with ^{82}Rb PET with only a 30-mCi injected dose. Finally, a three-dimensional display of gated ^{82}Rb PET images acquired during pharmacologic stress with adenosine is shown (**e**). Though gated myocardial perfusion SPECT images are acquired poststress, reflecting regional and global left ventricular function in the resting state, gated ^{82}Rb PET images are acquired during pharmacologic stress as well as at rest. As such, gated ^{82}Rb PET images provide an indirect evaluation of abnormal myocardial perfusion as reflected in regional wall motion abnormalities during stress, as opposed to poststress with SPECT. In this patient example, a surface rendering of end-diastolic and end-systolic images from gated adenosine ^{82}Rb PET is shown along with the time–activity curve. The left ventricular ejection fraction is calculated to be 36% during adenosine ^{82}Rb PET and 28% at rest. A postexercise gated SPECT left ventricular ejection fraction acquired in the same patient was calculated to be 32% [41]

Figure 4.32 presents experimental validation of ^{82}Rb for measuring myocardial blood flow. The kinetic model of ^{82}Rb is relatively "simple" because cellular trapping of ^{82}Rb is nonlinearly proportional to blood flow.

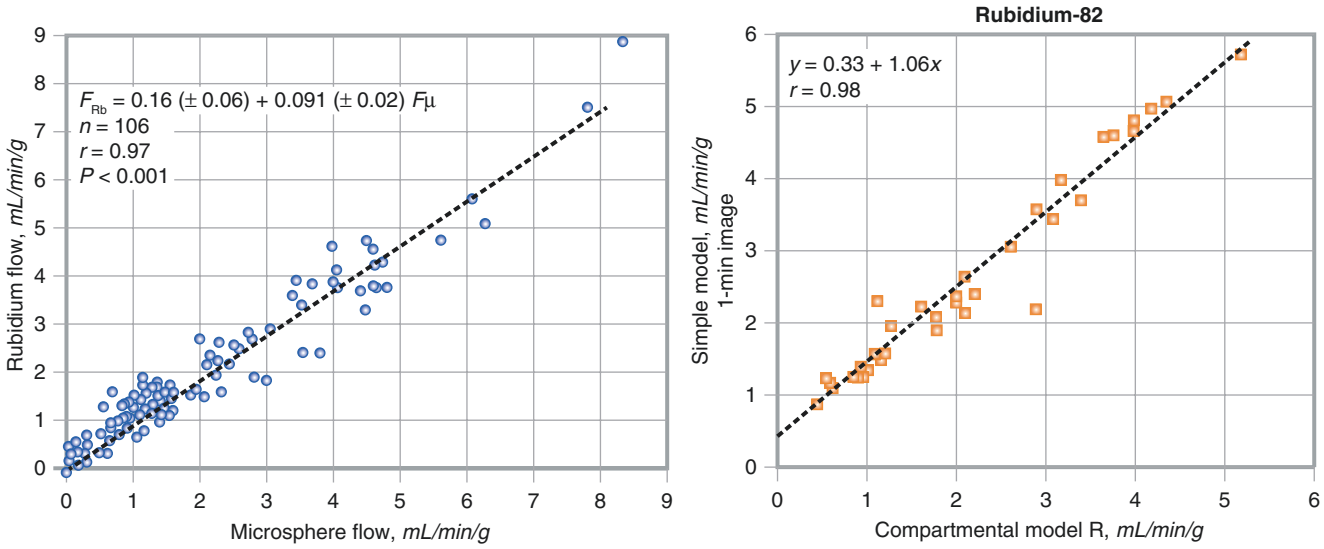

Fig. 4.32 Experimental validation of ^{82}Rb for measuring myocardial blood flow. The cellular trapping of ^{82}Rb is nonlinearly proportional to blood flow, making the kinetic model relatively "simple." (**a**) The initial verification of absolute myocardial perfusion with ^{82}Rb compared with microspheres is shown, measured by epicardial radiation detectors [42]. (**b**) Coronary flow reserve (CFR) measured by ^{82}Rb PET is validated using a "simple" flow model for flow-dependent ^{82}Rb extraction, compared with the more complex complete compartmental modeling, both having a comparable correlation with CFR measured by flowmeter [43]

PET myocardial perfusion images can reveal the severity and progression of coronary artery stenosis and coronary function, as shown in Fig. 4.33. Similarly, serial changes in PET perfusion images (Fig. 4.34) can be used to assess the response to treatment, predict outcomes, and provide insight into the progression or regression of coronary artery lesions and myocardial ischemia.

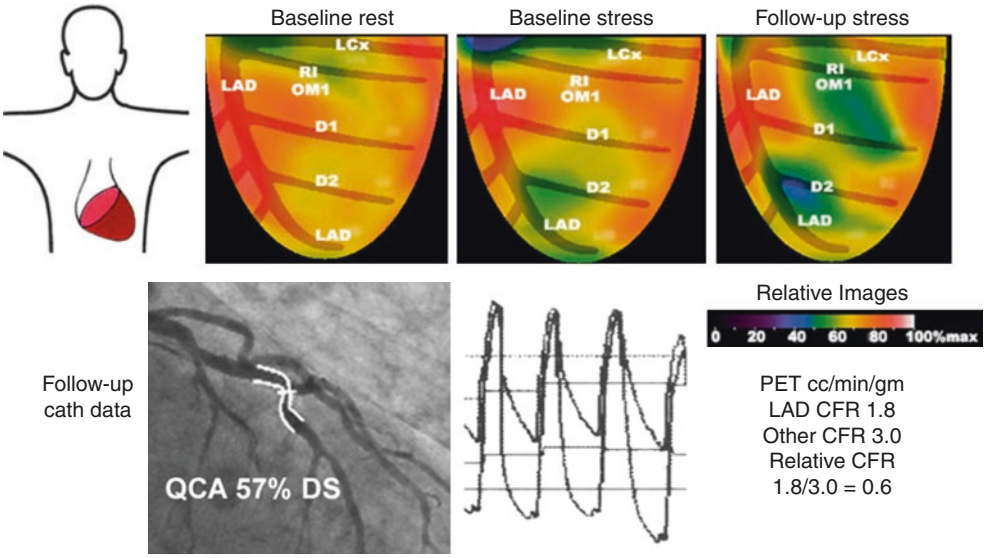

Fig. 4.33 Severity of anatomic coronary artery stenosis and coronary function. Relative uptake PET myocardial perfusion images are shown for a patient with known coronary artery disease and multiple risk factors; results at baseline (rest and stress) and 6 years later (follow-up stress) are shown. The follow-up PET study shows the progression of the stress-induced perfusion defect in the mid-left anterior descending (LAD) distribution (which was only 65% of the activity in the adjacent proximal areas of the heart) along with a new perfusion defect in the ramus intermedius or first obtuse marginal branch distribution. PET shows that the CFR in the distal LAD is reduced to 1.8, compared with an average of 3.0 in the rest of the heart proximally and 4.0 in healthy young volunteers. A coronary arteriogram shows concentric 57% mid-LAD stenosis by automated quantitative coronary arteriographic analysis (QCA); the fractional flow reserve (FFR) assessed by pressure wire measurements in the aorta and distal to the stenosis is 0.65. In view of concordant low CFR and FFR, a LAD stent was placed, with improvement in FFR to 0.92, indicating residual pressure gradient due to diffuse disease proximal to the stent. (From Gould [44]; with permission from Elsevier)

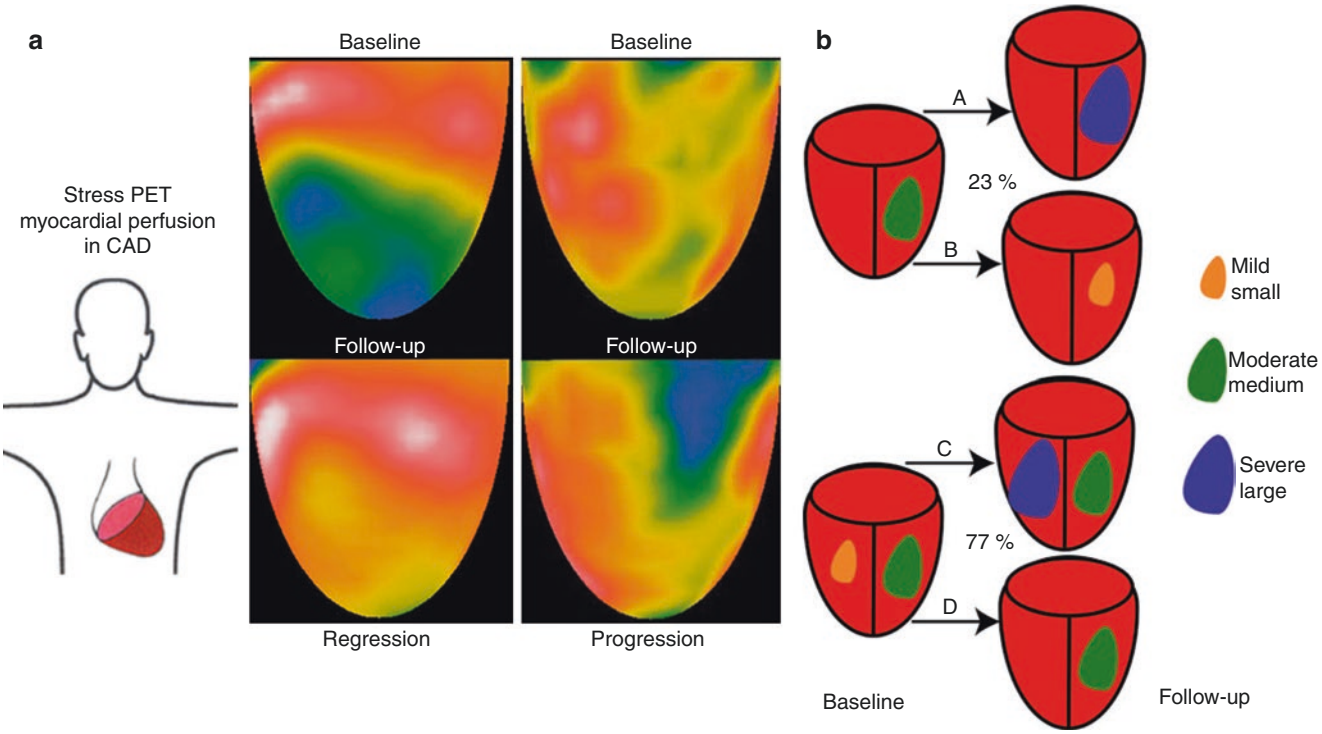

Fig. 4.34 Clinical impact of quantitative myocardial PET perfusion imaging. (**a**) Single views of stress PET relative perfusion images are shown for two different patients at baseline (*top row*) and follow-up (*bottom row*), one demonstrating regression and the other progression of coronary artery disease. (**b**) This schematic of stress PET images at baseline is compared with follow-up PET in various quadrant pairings. (From Gould [44]; with permission from Elsevier)

Figure 4.35 demonstrates the independent prognostic value of myocardial blood flow reserve (MFR) measurement by stress ^{82}Rb-PET in patients with myocardial ischemia. Patients shown to have impaired MFR had a higher incidence of major adverse cardiac events (MACE) at approximately 1 year of follow-up [45].

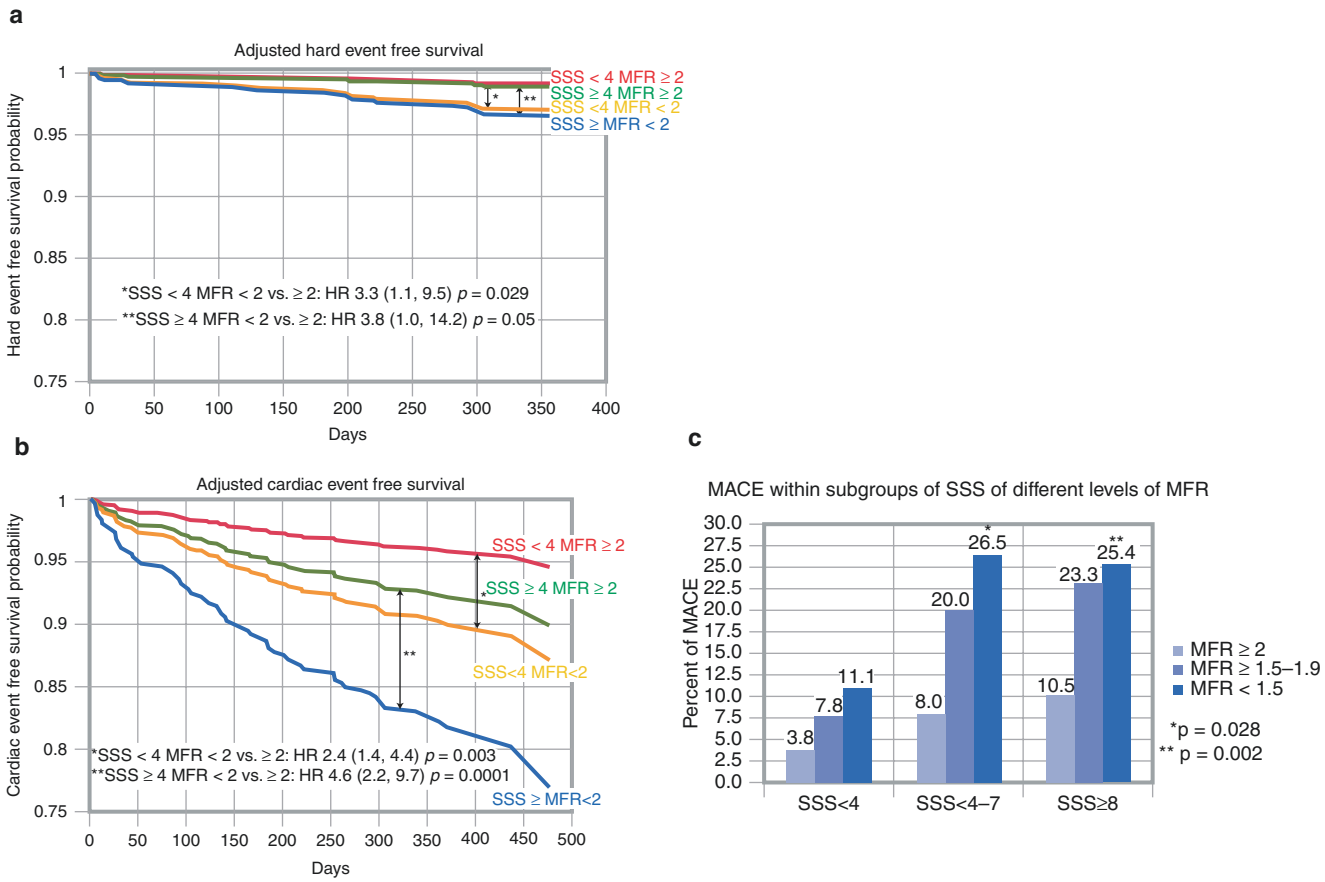

Fig. 4.35 Prognostic value of measurement by stress ^{82}Rb-PET. In a large cohort of patients referred for assessment of myocardial ischemia with ^{82}Rb-PET, the added and independent prognostic value of MFR was determined beyond the conventional relative myocardium radiotracer uptake on attenuation-corrected PET images. Patients with impaired ^{82}Rb MFR had a higher incidence of hard and major adverse cardiac events (MACE) (cardiac death, nonfatal myocardial infarction, late revascularization, or hospitalization for cardiac reasons) at approximately 1 year of follow-up. In the multivariable model analysis, ^{82}Rb MFR was an independent predictor of hard events (**a**) and MACE (**b**) over the summed stress score (SSS). MACE within subgroups of SSS for different levels of MFR is shown in (**c**). At any level of SSS, the prevalence of MACE is higher in patients with the lowest MFR (<1.5); among patients with overt ischemia, the difference from those with MFR ≥2 is statistically significant [45]

Another PET technique uses ^{15}O-water (Fig. 4.36), which is a freely diffusible tracer that correlates closely with perfusion as assessed by microspheres; its first-pass extraction fraction approaches unity. Because water can freely exchange across all normal tissue cells, the perfusable tissue fraction (PTF)—defined as the fractional volume of a given region of interest occupied by myocardium that is capable of exchanging water rapidly—should approach unity in normal myocardium and will be reduced in scarred myocardium.

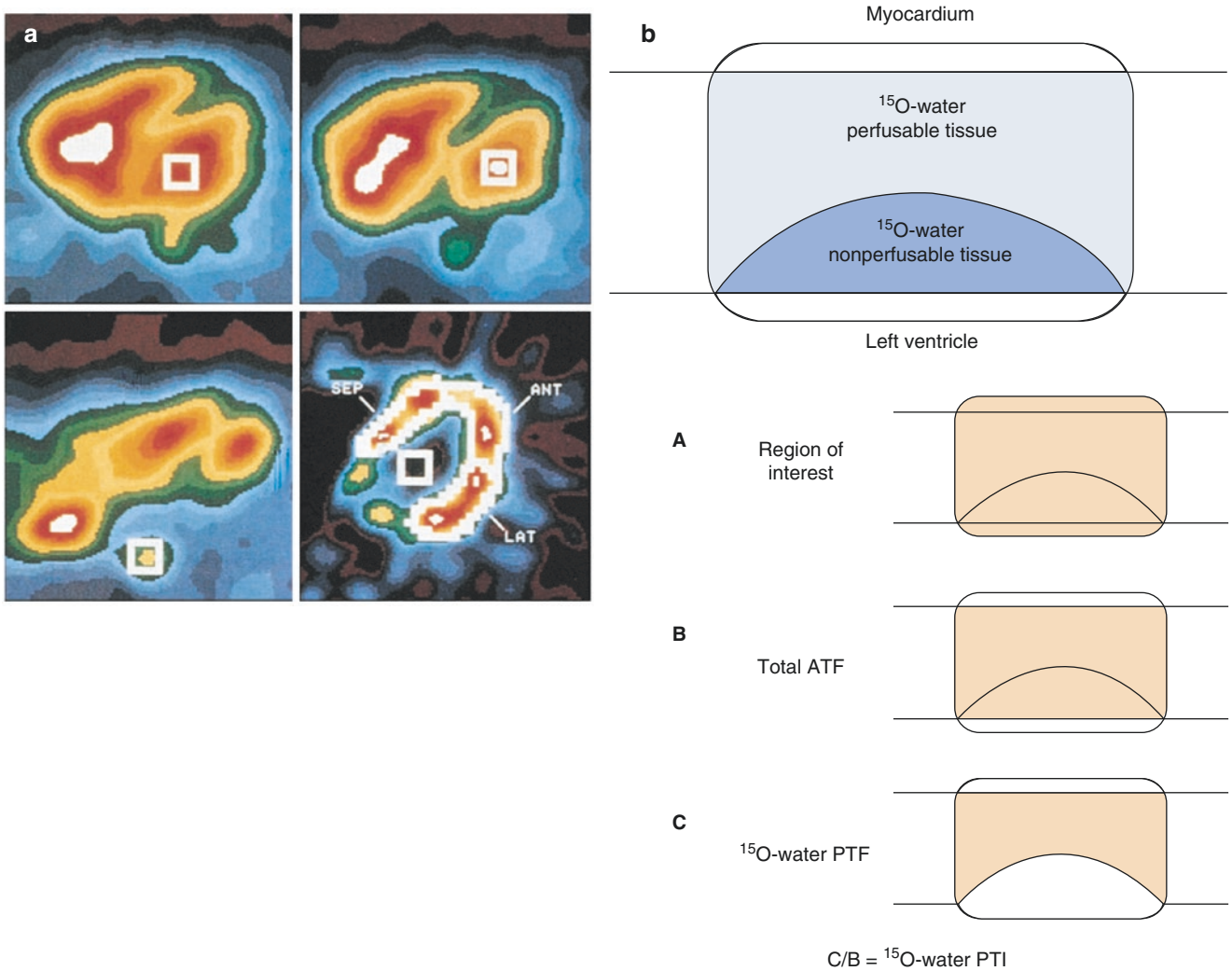

Fig. 4.36 PET techniques: ^{15}O-water. ^{15}O-water is a freely diffusible tracer that correlates closely with perfusion as assessed by microspheres, with a first-pass extraction fraction approaching unity. Because ^{15}O-water is in both the vascular space and myocardium, visualization of myocardial activity requires correction for activity in the vascular compartment. (**a**) Corrections for activity in the left atrium (*top left*), left ventricle (*top right*), and thoracic aorta (*bottom left*) are shown in a healthy patient after inhalation of 30–40 mCi of ^{15}O-carbon monoxide, which labels erythrocytes in vivo. The distribution of ^{15}O-water is shown in the left ventricular myocardium (*bottom right*) after correcting for vascular space. (**b**) The ability of ^{15}O-water to assess myocardial viability through modification of the blood flow information is shown. This method, termed *water perfusable tissue index* (PTI), is based on a measurement of perfusable tissue fraction (PTF) as a method to correct for the partial volume effects in ^{15}O-water studies [46]. PTF is defined as the fractional volume of a given region of interest occupied by myocardium that is capable of exchanging water rapidly. Using transmission and ^{15}O-blood pool images, the anatomic tissue fraction (ATF), a quantitative estimate of extravascular tissue density, is derived. The ratio of PTF to ATF thus represents the proportion of the extravascular tissue that is perfusable by ^{15}O-water. Because water can freely exchange across all normal tissue cells, the PTF should approach unity in normal myocardium and be reduced in scarred myocardium. A myocardial region of interest containing a mixture of ^{15}O-water perfusable and nonperfusable tissue is diagrammed. The volume of the region of interest is shown (*A*). ATF for the region of interest is produced by subtracting the blood pool (^{15}O-carbon monoxide) from the transmission images after normalizing the latter to tissue density (1.04 g/mL). The total ATF (*B*) represents the total extravascular tissue and contains both perfusable and nonperfusable tissue components. The ^{15}O-water PTF for the region of interest calculated from the ^{15}O-water data set identifies the mass of tissue within the region of interest that is capable of rapid trans-sarcolemmal exchange of water. Note that the nonperfusable or necrotic region is excluded from this parameter. The ^{15}O-water PTI is calculated by dividing ^{15}O-water PTF (*C*) by the total ATF (*B*) and represents the fraction of the total anatomic tissue that is perfusable by water. ANT—anterior; LAT—lateral; SEP—septal. (**a** *From* Bergmann et al. [47], with permission from Elsevier; **b** *From* Yamamoto et al. [48]; with permission from Wolters Kluwer)

The extractable perfusion tracer most commonly used with PET is ^{13}N-ammonia. At physiologic pH, ammonia is in its cationic form, with a physical half-life of 10 minutes. Myocardial distribution of ammonia is related inversely and nonlinearly to blood flow. Although the exact mechanism of ^{13}N-ammonia transport across the myocardial membrane has not been conclusively established, it has been suggested that ^{13}N-ammonia may cross cell membranes by passive diffusion or as ammonium ion ($^{13}NH+_4$) by the active sodium–potassium transport mechanism influenced by the concentration gradient across the cell membrane (Fig. 4.37). Once in the myocyte, myocardial retention of ^{13}N-ammonia involves predominantly the conversion of ^{13}N-ammonia and glutamic acid to ^{13}N-labeled glutamine mediated by ATP and glutamine synthetase. Hence, absolute quantification requires two- and three-compartment kinetic models that incorporate both extraction and retention rate constants. Quantification of ammonia is further complicated by the rapid degradation of ammonia, which occurs within 5 minutes after administration, producing metabolic intermediates, such as urea and glutamine, which are also extracted by the heart. Experimental studies suggest that the myocardial uptake of ammonia reflects absolute blood flows up to 2–2.5 mL/g/minute and plateaus at flows in the hyperemic range. In the clinical setting, 10–20 mCi of ^{13}N-ammonia is administered intravenously. Figure 4.38 shows an example of ^{13}N-ammonia PET and coronary angiography in a patient with coronary artery disease.

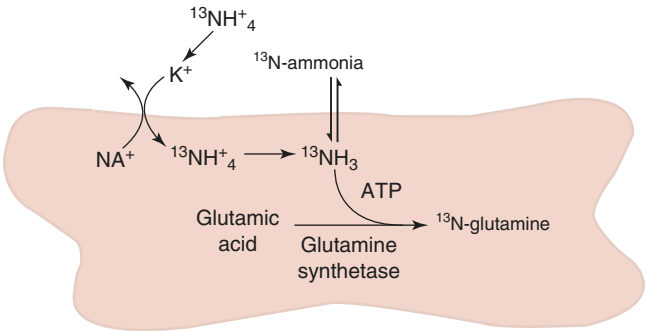

Fig. 4.37 PET techniques: ^{13}N-ammonia. It has been suggested that ^{13}N-ammonia may cross cell membranes by passive diffusion or as ammonium ion ($^{13}NH+_4$) by the active sodium–potassium transport mechanism influenced by the concentration gradient across the cell membrane. Once in the myocyte, myocardial retention of ^{13}N-ammonia involves predominantly the conversion of ^{13}N-ammonia and glutamic acid to ^{13}N-labeled glutamine mediated by ATP and glutamine synthetase

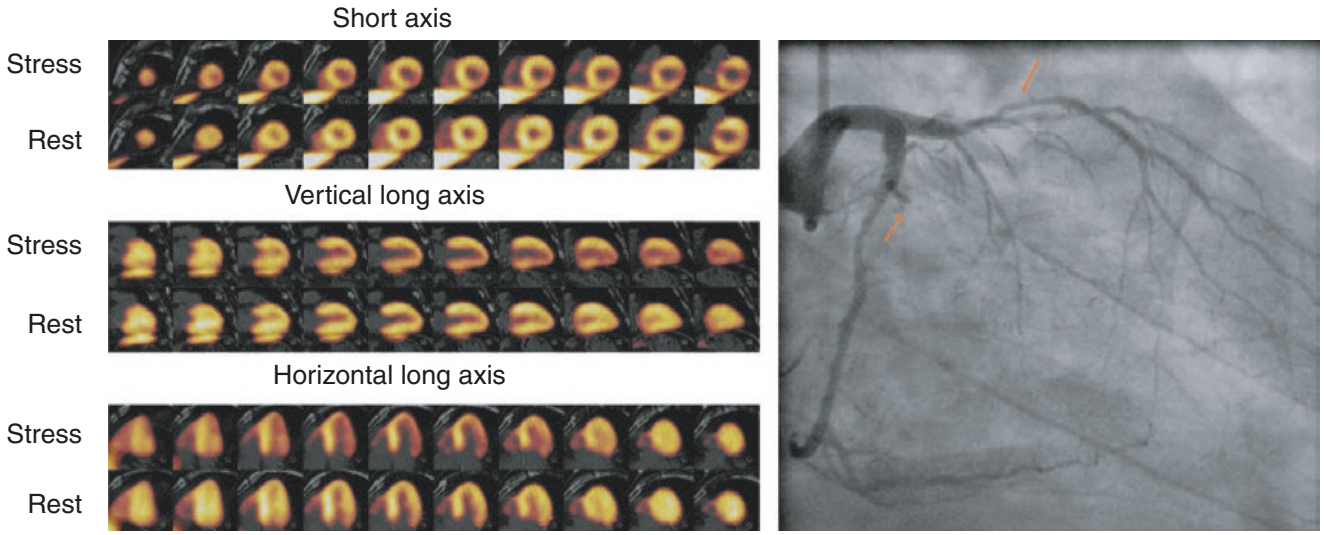

Fig. 4.38 ^{13}N-ammonia PET and coronary angiography in a patient with coronary artery disease [39]. These stress and rest ^{13}N-ammonia PET images of the heart in short-axis, vertical long-axis, and horizontal long-axis slices are shown from a 62-year-old patient who has type 2 diabetes. The stress images demonstrate a moderately decreased perfusion defect involving the lateral region of the left ventricle, extending to the inferolateral region—a defect that is completely reversible in rest images. The corresponding coronary angiography shows an occluded marginal branch of the left circumflex artery (*left arrow*), with diffuse 50% stenosis of the proximal LAD (*right arrow*) and a 50% stenosis in the mid-RCA (*not shown*). (*From* Schindler et al. [40]; with permission from Wiley)

The interplay between blood flow and metabolism in the extraction and retention of ^{13}N-ammonia is complex, as seen in Fig. 4.39. The early extraction phase of freely diffusible ^{13}N-ammonia reflects blood flow, whereas the later, slow-turnover phase reflects the metabolic trapping of ^{13}N-ammonia. Because the extent of ^{13}N-ammonia metabolism may depend on the ATP state of the myocyte, intracellular levels of ^{13}N-ammonia may reflect cellular viability, and late ammonia uptake (metabolic trapping) is a significantly better predictor of functional improvement after revascularization than is absolute blood flow. Thus, beyond ammonia's value as a perfusion tracer, late ammonia images provide important insight regarding cell membrane integrity and myocardial viability [49].

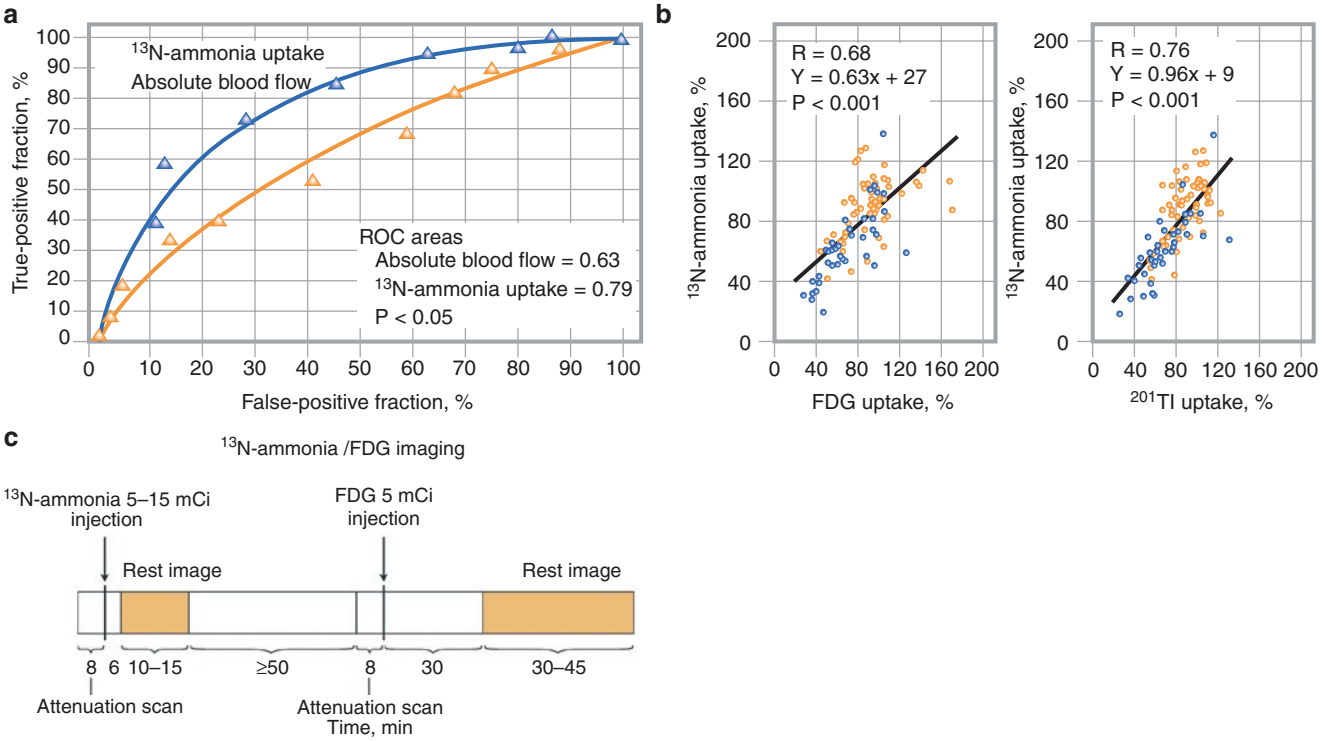

Fig. 4.39 Mechanism of ^{13}N-ammonia uptake. The interplay between blood flow and metabolism in the extraction and retention of ^{13}N-ammonia is complex. The early extraction phase of freely diffusible ^{13}N-ammonia reflects blood flow, whereas the later, slow-turnover phase reflects the metabolic trapping of ^{13}N-ammonia. In experimental animals, several investigators have shown that the myocardial extraction and retention of ^{13}N-ammonia are related not only to regional blood flow but also to myocardial oxygenation and metabolism. Under hypoxic or ischemic conditions, the reduction of intracellular ATP to concentrations in the range of the K_m for the enzyme–ATP complex could reduce intracellular ^{13}N-ammonia metabolism by glutamine synthetase. Because the extent of ^{13}N-ammonia metabolism may depend on the ATP state of the myocyte, intracellular levels of ^{13}N-ammonia may reflect cellular viability. (**a**) In patients with chronic coronary artery disease and left ventricular dysfunction, receiver-operating characteristic (ROC) curves were used to compare the abilities of late ammonia uptake (final 10–15 minutes of image acquisition) and absolute blood flow (early extraction phase, approximately 3 minutes after injection) to predict the functional improvement of asynergic regions after revascularization. The results show that late ammonia uptake (metabolic trapping) is significantly better than absolute blood flow as a predictor of functional improvement after revascularization. (**b**) There is a linear relationship between percent late ammonia uptake and [^{18}F]-fluorodeoxyglucose (FDG) uptake (*left*) and between ^{201}Tl uptake on redistribution imaging (*right*) in reversible (*orange circles*) and irreversible (*blue circles*) asynergic regions after revascularization. (**c**) Sequence and timing of ^{13}N-ammonia and FDG PET imaging for the assessment of myocardial viability. Beyond ammonia's value as a perfusion tracer, late ammonia images provide important insight regarding cell membrane integrity and myocardial viability [49]

PET approaches for the assessment of regional myocardial blood flow in mL/g/minute entail the intravenous injection of a positron-emitting perfusion tracer, such as rubidium-82, ^{13}N-ammonia, or ^{15}O-water, and the dynamic acquisition of images of the radiotracer passing through the central circulatory system to its extraction and retention in the left ventricular myocardium. Tracer kinetic models (one to three compartments) and operational equations are then applied to correct for the physical decay of the radioisotope, partial volume–related underestimation of the true myocardial tissue concentrations by assuming a uniform myocardial wall thickness of 1 cm, and spillover of radioactivity between the left ventricular blood pool and myocardium, to yield regional myocardial blood flows in absolute terms, mL/g/minute. The relative distribution of the radiotracer in the myocardium can also be assessed visually or semiquantitatively (as percent uptake relative to a reference region) from the final static image of the myocardium, obtained from the last (e.g., 900 s) frame of the PET image series, which can be displayed as a polar map. Table 4.7 summarizes the characteristics of the common PET myocardial perfusion tracers [38].

Characteristics	Rubidium-82	^{13}N-ammonia	^{15}O-Water
Half-life	78 s	9.8 minutes	2.4 minutes
Extraction	≈60%	≈80%	≈95%
Cyclotron onsite	No	Yes	Yes
Data acquisition	Dynamic, static, gated	Dynamic, static, gated	Dynamic
Scan duration	6 minutes	20 minutes	5 minutes
Dose-2D	40–60 mCi	15–25 mCi	40 mCi
Dose-3D	15–20 mCi	15 mCi	10 mCi
	30–40 mCi 3D		
	LSO		
Interval between doses	10 minutes	45 minutes	7 minutes
Image interpretation	Yes	Yes	No
Image quality	Good	Excellent	N/A

2D two-dimensional, *3D* three-dimensional, *LSO* Lutetium oxyorthosilicate

Table 4.7 PET myocardial perfusion tracers and image acquisition

Table 4.8 reviews a number of studies of the identification of flow-limiting coronary artery lesions by PET. Similar to SPECT, the identification of stress-induced scintigraphic perfusion defects by PET imaging provides important diagnostic and prognostic information. Unlike SPECT imaging, however, soft tissue attenuation correction with PET imaging is reliable and accurate. This accurate attenuation correction, in concert with the higher spatial resolution, may explain the 10% higher diagnostic accuracy of PET when compared with conventional SPECT imaging for the detection of flow-limiting coronary artery lesions. The advantages of PET imaging, however, pertain not only to the high spatial and depth-independent resolution but also to the ability to quantify the radiotracer uptake in the myocardial tissue and to assess rapid alterations of radiotracer activity concentrations in the arterial blood and myocardium, owing to a high temporal resolution in seconds. The latter advantages of PET imaging, combined with tracer kinetic compartment models, afford the noninvasive assessment of myocardial blood flow in absolute terms.

Year	Author	Radiotracer	Prior MI, %	Sensitivity, %	Specificity, %
2008	Esteves et al.	^{82}Rubidium	0	90 (36/40)	83 (10/12)
2007	Sampson et al.	^{82}Rubidium	0	93 (41/44)	83 (48/58)
1992	Marwick et al.	^{82}Rubidium	49	90 (63/70)	100 (4/4)
1992	Grover-McKay et al.	^{82}Rubidium	13	100 (16/16)	73 (11/15)
1991	Stewart et al.	^{82}Rubidium	42	83 (50/60)	86 (18/21)
1990	Go et al.	^{82}Rubidium	47	93 (142/152)	78 (39/50)
1989	Demer et al.	^{82}Rubidium, ^{13}N-ammonia	34	83 (126/152)	95 (39/41)
1988	Tamaki et al.	^{13}N-ammonia	75	98 (47/48)	100 (3/3)
1986	Gould et al.	^{82}Rubidium, ^{13}N-ammonia	Unknown	95 (21/22)	100 (9/9)
1982	Schelbert et al.	^{13}N-ammonia	0	97 (31/32)	100 (11/11)
Total				92 (573/636)	90 (192/224)

Table 4.8 Identification of flow-limiting coronary artery lesions by PET myocardial perfusion tracers

^{82}Rb (Table 4.9) is a generator-produced, short-lived, positron-emitting cation with biologic properties that are similar to potassium and ^{201}Tl. As with potassium and ^{201}Tl, the intracellular uptake of ^{82}Rb across the sarcolemmal membrane reflects active cation transport via the Na–K ATPase transport system. In patients with chronic coronary artery disease, myocardial uptake of ^{82}Rb is preserved in viable regions and is severely reduced in scarred regions. In the setting of acute myocardial injury and reperfusion, the initial uptake of ^{82}Rb reflects blood flow.

Positron-emitting cation with biologic properties similar to potassium
Emits two γ-rays, 511 keV each, with a short physical half-life of 75 s
Transported across the sarcolemmal membrane via the Na–K ATPase system
Initial uptake reflects myocardial blood flow
Kinetics of washout phase may be used as an index of viability

Table 4.9 PET techniques: ^{82}Rb

The improved diagnostic accuracy of PET over SPECT for detecting coronary artery disease (CAD) can be attributed to the higher photon energy of PET radiotracers, as well as to the improved resolution and intrinsic attenuation correction of PET cameras. The latter has enabled PET to assess absolute myocardial blood flow, from which coronary flow reserve (CFR) can be quantified noninvasively. However, outcome data with PET in patients with CAD are scarce. Figure 4.40 illustrates such outcome data In a group of patients with suspected myocardial ischemia who underwent ^{13}N-ammonia PET [50]. Beyond detection of CAD, ^{13}N-ammonia PET perfusion and CFR data are strong predictors of adverse outcome. CFR is an independent predictor of adverse outcome. It provides a 3-year "warranty" period of event-free survival for patients with normal CFR and normal PET perfusion. Conversely, in patients with abnormal perfusion, an impaired CFR has added value for predicting adverse outcomes.

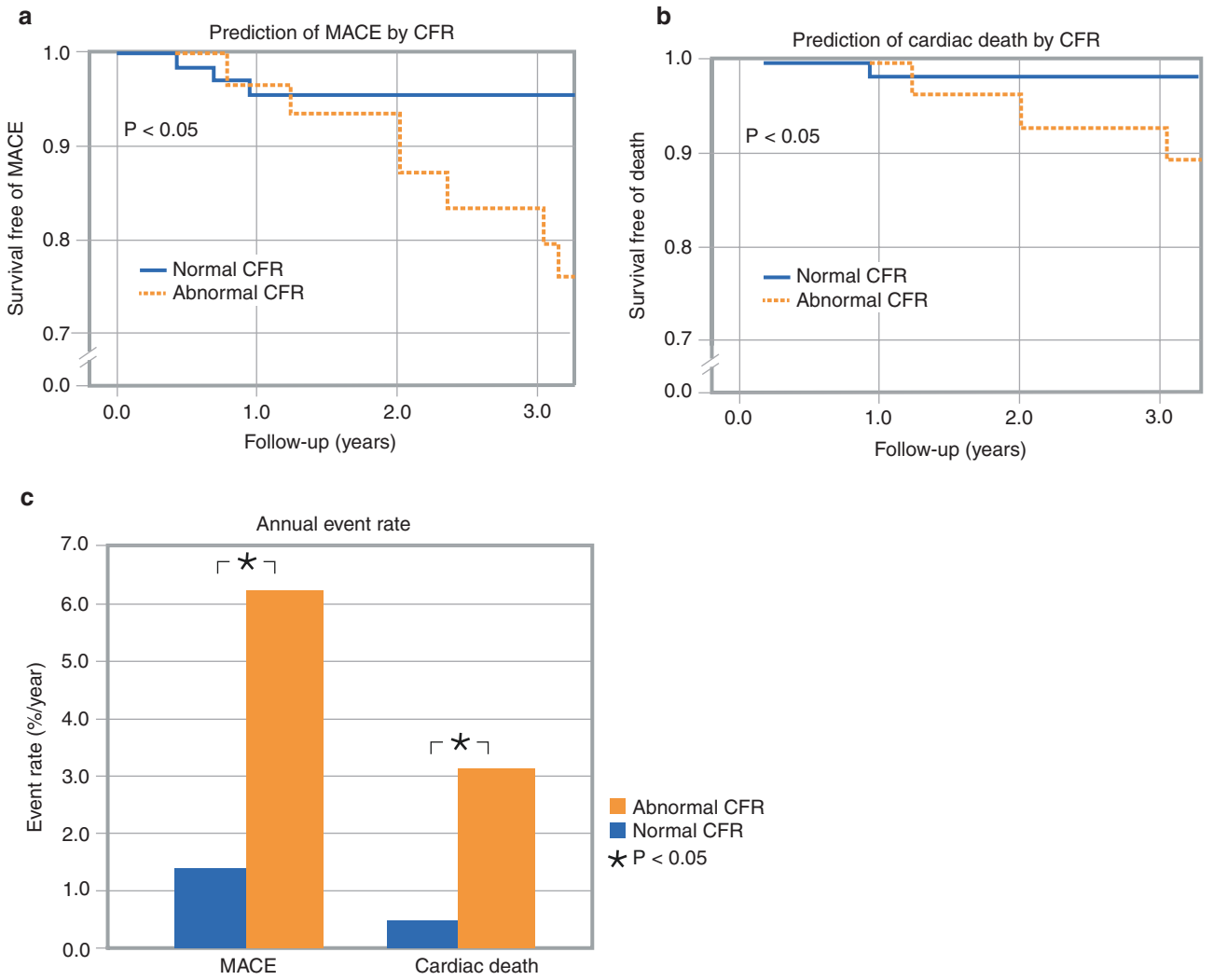

Fig. 4.40 Predictive value of major adverse cardiac events, including cardiac death, by stress ^{13}N-ammonia PET. Herzog et al. [50] assessed the long-term prognostic value of CFR over a mean of 5.4 years in patients with suspected myocardial ischemia who underwent ^{13}N-ammonia PET. Major adverse cardiac events (MACE) (cardiac death, nonfatal myocardial infarction, late revascularization, or hospitalization for cardiac reasons) occurred in 34% of the patients. Abnormal PET perfusion was associated with a higher incidence of MACE ($P < 0.001$) and cardiac death ($P < 0.05$). In patients with normal perfusion, abnormal CFR was independently associated with a higher annual event rate over 3 years compared with normal CFR for MACE (1.4% vs. 6.3%; $P < 0.05$) (**a**) and cardiac death (0.5% vs. 3.1%; $P < 0.05$) (**b**). This is reflected by the higher annual event rate (%/year) in abnormal CFR (**c**). In patients exhibiting abnormal perfusion, CFR remained predictive throughout the 10-year follow-up ($P < 0.001$). Beyond detection of CAD, ^{13}N-ammonia PET perfusion and CFR data are strong predictors of adverse outcome [50]

References

1. Cerqueira MD, Weissman NJ, Dilsizian V, Jacobs AK, Kaul S, Laskey WK, et al. American Heart Association Writing Group on Myocardial Segmentation and Registration for Cardiac Imaging. Standardized myocardial segmentation and nomenclature for tomographic imaging of the heart. A statement for healthcare professionals from the Cardiac Imaging Committee of the Council on Clinical Cardiology of the American Heart Association. Circulation. 2002;105:539–42.
2. Dilsizian V, Rocco TP, Freedman NM, Leon MB, Bonow RO. Enhanced detection of ischemic but viable myocardium by the reinjection of thallium after stress-redistribution imaging. N Engl J Med. 1990;323:141–6.
3. Maddahi J, Van Train K, Prigent F, Garcia EV, Friedman J, Ostrzega E, Berman D. Quantitative single photon emission computed thallium-201 tomography for detection and localization of coronary artery disease: optimization and prospective validation of a new technique. J Am Coll Cardiol. 1989;14:1689–99.
4. Fintel DJ, Links JM, Brinker JA, Frank TL, Parker M, Becker LC. Improved diagnostic performance of exercise thallium-201 single photon emission computed tomography over planar imaging in the diagnosis of coronary artery disease: a receiver operating characteristic analysis. J Am Coll Cardiol. 1989;13:600–12.
5. Iskandrian AS, Heo J, Kong B, Lyons E. Effect of exercise level on the ability of thallium-201 tomographic imaging in detecting coronary artery disease: analysis of 461 patients. J Am Coll Cardiol. 1989;14:1477–86.
6. Go RT, Marwick TH, MacIntyre WJ, Saha GB, Neumann DR, Underwood DA, Simpfendorfer CC. A prospective comparison of rubidium-82 PET and thallium-201 SPECT myocardial perfusion imaging utilizing a single dipyridamole stress in the diagnosis of coronary artery disease. J Nucl Med. 1990;31:1899–905.
7. Mahmarian JJ, Boyce TM, Goldberg RK, Cocanougher MK, Roberts R, Verani MS. Quantitative exercise thallium-201 single photo emission computed tomography for the enhanced diagnosis of ischemic heart disease. J Am Coll Cardiol. 1990;15:318–29.
8. Van Train KF, Maddahi J, Berman DS, Kiat H, Areeda J, Prigent F, Friedman J. Quantitative analysis of tomographic stress thallium-201 myocardial scintigrams: a multicenter trial. J Nucl Med. 1990;31:1168–79.
9. Kiat H, Maddahi J, Roy LT, Van Train K, Friedman J, Resser K, Berman DS. Comparison of technetium 99m methoxy isobutyl isonitrile and thallium 201 for evaluation of coronary artery disease by planar and tomographic methods. Am Heart J. 1989;117:1–11.
10. Iskandrian AS, Heo J, Kong B, Lyons E, Marsch S. Use of technetium-99m isonitrile (RP-30A) in assessing left ventricular perfusion and function at rest and during exercise in coronary artery disease, and comparison with coronary arteriography and exercise thallium-201 SPECT imaging. Am J Cardiol. 1989;64:270–5.
11. Kahn JK, McGhie I, Akers MS, Sills MN, Faber TL, Kulkarni PV, et al. Quantitative rotational tomography with 201Tl and 99mTc 2-methoxy-isobutyl-isonitrile. A direct comparison in normal individuals and patients with coronary artery disease. Circulation. 1989;79:1282–93.
12. Solot G, Hermans J, Merlo P, Chaudron JM, Luwaert R, Cheron P, et al. Correlation of 99Tcm-sestamibi SPECT with coronary angiography in general hospital practice. Nucl Med Commun. 1993;14:23–9.
13. Van Train KF, Garcia EV, Maddahi J, Areeda J, Cooke CD, Kiat H, et al. Multicenter trial validation for quantitative analysis of same-day rest-stress technetium-99m-sestamibi myocardial tomograms. J Nucl Med. 1994;35:609–18.
14. Azzarelli S, Galassi AR, Foti R, Mammana C, Musumeci S, Giuffrida G, Tamburino C. Accuracy of 99m-tetrofosmin myocardial tomography in the evaluation of coronary artery disease. J Nucl Cardiol. 1999;6:183–9.
15. Ritchie JL, Bateman TM, Bonow RO, Crawford MH, Gibbons RJ, Hall RJ, et al. Guidelines for clinical use of cardiac radionuclide imaging. Report of the American College of Cardiology/American Heart Association Task Force on Assessment of Diagnostic and Therapeutic Cardiovascular Procedures (Committee on Radionuclide Imaging), developed in collaboration with the American Society of Nuclear Cardiology. J Am Coll Cardiol. 1995;25:521–47.
16. Gibson RS, Watson DD, Craddock GB, Crampton RS, Kaiser DL, Denny MJ, Beller GA. Predication of cardiac events after uncomplicated myocardial infarction: a prospective study comparing predischarge exercise thallium-201 scintigraphy and coronary angiography. Circulation. 1983;68:321–36.
17. Kiat H, Berman DS, Maddahi J, De Yang L, Van Train K, Rozanski A, Friedman J. Late reversibility of tomographic myocardial thallium-201 defects: an accurate marker of myocardial viability. J Am Coll Cardiol. 1988;12:1456–63.
18. Cloninger KG, DePuey EG, Garcia EV, Roubin GS, Robbins WL, Nody A, et al. Incomplete redistribution in delayed thallium-201 single photon emission computed tomographic (SPECT) images: an overestimation of myocardial scarring. J Am Coll Cardiol. 1988;12:955–63.
19. Dilsizian V. Thallium-201 scintigraphy: experience of two decades. In: Dilsizian V, editor. Myocardial viability: a clinical and scientific treatise. Armonk: Futura; 2000. p. 265–313.
20. Zimmermann R, Mall G, Rauch B, Zimmer G, Gabel M, Zehelein J, et al. Residual 201Tl activity in irreversible defects as a marker of myocardial viability. Clinicopathological study. Circulation. 1995;91:1016–21.
21. Kayden DS, Sigal S, Soufer R, Mattera J, Zaret BL, Wackers FJ. Thallium-201 for assessment of myocardial viability: quantitative comparison of 24-hour redistribution imaging with imaging after reinjection at rest. J Am Coll Cardiol. 1991;18:1480–6.
22. Kitsiou AN, Srinivasan G, Quyyumi AA, Summers RM, Bacharach SL, Dilsizian V. Stress-induced reversible and mild-to-moderate irreversible thallium defects: are they equally accurate for predicting recovery of regional left ventricular function after revascularization? Circulation. 1998;98:501–8.
23. Petretta M, Cuocolo A, Bonaduce D, Nicolai E, Cardei S, Berardino S, et al. Prognostic value of thallium reinjection after stress-redistribution imaging in patients with previous myocardial infarction and left ventricular dysfunction. J Nucl Med. 1997;38:195–200.
24. Arrighi JA, Dilsizian V. Identification of viable, nonfunctioning myocardium. In: Brown DL, editor. Cardiac intensive care. Philadelphia: WB Saunders; 1998. p. 307–27.
25. Gioia G, Milan E, Giubbini R, DePace N, Heo J, Iskandrian AS. Prognostic value of tomographic rest-redistribution thallium-201 imaging in medically treated patients with coronary artery disease and left ventricular dysfunction. J Nucl Cardiol. 1996;3:150–6.
26. Gioia G, Powers J, Heo J, Iskandrian AS. Prognostic value of rest-redistribution tomographic thallium-201 imaging in ischemic cardiomyopathy. Am J Cardiol. 1995;75:759–62.
27. Pagley PR, Beller GA, Watson DD, Gimple LW, Ragosta M. Improved outcome after coronary bypass surgery in patients with ischemic cardiomyopathy and residual myocardial viability. Circulation. 1997;96:793–800.
28. Piwnica-Worms D, Chiu ML, Kronauge JF. Divergent kinetics of 201Tl and 99mTc-SESTAMIBI in cultured chick ventricular myocytes during ATP depletion. Circulation. 1992;85:1531–41.
29. Narahara KA, Villanueva-Meyer J, Thompson CJ, Brizendine M, Mena I. Comparison of thallium-201 and technetium-99m hexakis 2-methoxyisobutyl isonitrile single-photon emission computed tomography for estimating the extent of myocardial

ischemia and infarction in coronary artery disease. Am J Cardiol. 1990;66:1438–44.
30. Leon AR, Eisner RL, Martin SE, Schmarkey LS, Aaron AM, Boyers AS, et al. Comparison of single-photon emission computed tomographic (SPECT) myocardial perfusion imaging with thallium-201 and technetium-99m sestamibi in dogs. J Am Coll Cardiol. 1992;20:1612–25.
31. Li QS, Solot G, Frank TL, Wagner HN Jr, Becker LC. Myocardial redistribution of technetium-99m-methoxyisobutyl isonitrile (SESTAMIBI). J Nucl Med. 1990;31:1069–76.
32. Dilsizian V, Arrighi JA, Diodati JG, Quyyumi AA, Alavi K, Bacharach SL, et al. Myocardial viability in patients with chronic coronary artery disease: comparison of 99mTc-sestamibi with thallium reinjection and [18F]fluorodeoxyglucose. Circulation. 1994;89:578–87.
33. Franceschi M, Guimond J, Zimmerman RE, Picard MV, English RJ, Carvalho PA, et al. Myocardial clearance of Tc-99m hexakis-2-methoxy-2-methylpropyl isonitrile (MIBI) in patients with coronary artery disease. Clin Nucl Med. 1990;15:307–12.
34. Bisi G, Sciagrà R, Santoro GM, Rossi V, Fazzini PF. Technetium-99m-sestamibi imaging with nitrate infusion to detect viable hibernating myocardium and predict postrevascularization recovery. J Nucl Med. 1995;36:1994–2000.
35. Mehry Y, Latour JG, Arsenault A, Rousseau G. Effect of coronary reperfusion on technetium-99m methoxyisobutylisonitrile uptake by viable and necrotic myocardium in the dog. Eur J Nucl Med. 1992;19:503–10.
36. Udelson JE, Coleman PS, Metherall J, Pandian NG, Gomez AR, Griffith JL, et al. Predicting recovery of severe regional ventricular dysfunction: comparison of resting scintigraphy with 201Tl and 99mTc-sestamibi. Circulation. 1994;89:2552–61.
37. Delbeke D, Videlefsky S, Patton JA, Campbell MG, Martin WH, Ohana I, Sandler MP. Rest myocardial perfusion/metabolism imaging using simultaneous dual-isotope acquisition SPECT with technetium-99m-MIBI/fluorine-18-FDG. J Nucl Med. 1995;36:2110–9.
38. Dilsizian V, Bacharach SL, Beanlands SR, Bergmann SR, Delbeke D, Dorbala S, Gropler RJ, Knuuti J, Schelbert H, Travin M. ASNC Imaging Guidelines/SNMMI Procedure Standard for Positron Emission Tomography (PET) Nuclear Cardiology Procedures. J Nucl Cardiol 2016;23(5):1187–226.
39. Schindler TH, Dilsizian V. Coronary Microvascular Dysfunction: Clinical Considerations and Noninvasive Diagnosis. J Am Coll Cardiol Img 2020;13:140–55.
40. Schindler TH, Valenta I, Dilsizian V. PET assessment of myocardial perfusion. In: Dilsizian V, Pohost GM, editors. Cardiac CT, PET, and MR. 2nd ed. Chichester: Wiley-Blackwell; 2009. p. 95–117.
41. Lodge MA, Braess H, Mahmoud F, Suh J, Englar N, Geyser-Stoops S, et al. Developments in nuclear cardiology: transition from SPECT to PET/CT. J Invasive Cardiol. 2005;17:491–6.
42. Goldstein RA, Mullami NA, Fisher D, Marani S, Gould K, O'Brien HA. Myocardial perfusion with rubidium-82. II. The effects of metabolic and pharmacologic interventions. J Nucl Med. 1983;24:907–15.
43. Yoshida K, Mullami NA, Gould KL. Coronary flow and flow reserve by PET simplified for clinical applications using rubidium-82 or nitrogen-13-ammonia. J Nucl Med. 1996;37:1701–12.
44. Gould K. Does coronary flow trump coronary anatomy? JACC Cardiovasc Imaging. 2009;2:1009–23.
45. Ziadi MC, DeKemp RA, Williams KA, Guo A, Chow BJ, Renaud JM, et al. Impaired myocardial flow reserve on rubidium-82 positron emission tomography imaging predicts adverse outcomes in patients assessed for myocardial ischemia. J Am Coll Cardiol. 2011;58:740–8.
46. Iida H, Rhodes CG, de Silva R, Yamamoto Y, Araujo LI, Maseri A, Jones T. Myocardial tissue fraction: correction for partial volume effects and measure of tissue viability. J Nucl Med. 1991;32:2169–75.
47. Bergmann SR, Herrero P, Markham J, Weinheimer CJ, Walsh MN. Noninvasive quantitation of myocardial blood flow in human subjects with oxygen-15-labeled water and positron emission tomography. J Am Coll Cardiol. 1989;14:639–52.
48. Yamamoto Y, de Silva R, Rhodes CG, Araujo LI, Iida H, Rechavia E, et al. A new strategy for the assessment of viable myocardium and regional myocardial blood flow using 15O-water and dynamic positron emission tomography. Circulation. 1992;86:167–78.
49. Kitsiou AN, Bacharach SL, Bartlett ML, Srinivasan G, Summers RM, Quyyumi AA, Dilsizian V. 13N-ammonia myocardial blood flow and uptake: relation to functional outcome of asynergic regions after revascularization. J Am Coll Cardiol. 1999;33:678–86.
50. Herzog BA, Husmann L, Valenta I, Gaemperli O, Siegrist PT, Tay FM, et al. Long-term prognostic value of 13N-ammonia myocardial perfusion positron emission tomography. J Am Coll Cardiol. 2009;54:150–6.